

A reaction-diffusion model for the transmission dynamics of the Coronavirus pandemic with reinfection and vaccination process

HAMADJAM ABBOUBAKAR^{1,*,\dagger}, REINHARD RACKE^{2,\ddagger}, and NICOLAS SCHLOSSER^{3,\ddagger}

^{*} *University of Ngaoundéré, University Institute of Technology, Department of Computer Engineering, P.O. Box 455, Ngaoundéré, Cameroon.*

^{\dagger} *University of Konstanz, Department of Mathematics and Statistics, P.O. Box 78457 Konstanz, Germany*

Abstract

This work aims at deriving and analysing a reaction-diffusion model for the transmission dynamics of the Coronavirus (COVID-19) which takes into account the reinfection and the vaccination process, and to compare it with the ODE model. After formulating the time-dependent ODE model, we compute the control reproduction number \mathcal{R}_c and prove the global stability of the disease-free equilibrium whenever $\mathcal{R}_c < 1$. We also demonstrate that if $\mathcal{R}_c > 1$, the disease-free equilibrium becomes unstable and coexists with at least one endemic equilibrium point. We then use data from Germany to calibrate our model and estimate some model parameters. We find that $\mathcal{R}_c \approx 1.13$ expressing that the disease persists in the population. To determine key parameters which influence the model dynamics, we perform global sensitivity analysis by computing partial rank correlation coefficients between model parameters and the control reproduction number (respectively model state variables). After that, we include in the previous model the mobility in space by transforming it into a reaction-diffusion PDE model. For this last initial value boundary problem (IVBP), we prove the non-negativity, existence, and uniqueness of solutions. We also prove the local and global stability of the disease-free equilibrium whenever $\mathcal{R}_c < 1$, and the fact that $\mathcal{R}_c > 1$ implies the instability of the DFE and its coexistence with at least one endemic equilibrium point. To validate our theoretical results, we perform numerous numerical simulations. We then compare the ODE model with the PDE model.

Key words: Covid-19, Reaction-diffusion model, Control reproduction number, Asymptotic stability, Model calibration, Sensitivity analysis, Partial Rank Correlation Coefficient.

AMS Classification: 92D30, 34A34, 34B15, 34C60, 35A01, 35A02.

1 Introduction

The Covid-19 pandemic started in 2019, see [21, 36, 34, 48] for the development and measurements of containment. May 2021 is the start date of vaccination in several countries around the world [46].

Since the beginning of the Covid-19 pandemic, several mathematical models were formulated and studied to predict the future of the disease, as well as the efficiency of control measures (see [5, 10, 22, 25, 33, 38] and the references therein). Some authors have worked on time-space models, also called reaction-diffusion models [6, 7, 9, 15, 18, 26, 29, 43, 49]. In [6], Ahmed et

¹email: abboubakarhamadjam@yahoo.fr or h.abboubakar@gmail.com

²email: reinhard.racke@uni-konstanz.de

³email: Nicolas.schlosser@uni-konstanz.de

al. formulated a SAIR reaction-diffusion model with nonlinear incidence rates in a constant population. Brusset et *al.* in [7] formulated a SIS reaction-diffusion model to represent how the geographic spread of the pandemic, by reducing the workers' participation to economic life, undermines the ability of firms and as a result the entire supply networks to satisfy customers' demands. An SI reaction-diffusion model with cross-diffusion is formulated and studied in [9] by Cherniha and Davydovych using the Lie symmetry method. In [15], Fitzgibbon et *al.* developed a dynamic model of an evolving epidemic in a spatially inhomogeneous environment. They analyzed it to predict the outbreak and spatio-temporal spread of the COVID-19 epidemic in Brazil. To take into account the non-local Covid-19 transmission due to the fact that people often travel long distances in short periods of time, Grave et *al.* in [18] combined a network structure within a reaction-diffusion PDE system. They defined the transfer network, the transfer operator, the donor operator, and the receiver operator. Kevrekidis et *al.* [26] formulated and studied an SEAIHR reaction-diffusion model with Greece and Andalusia as case examples. Youcef Mammeri in [29] formulated and studied a SEAIR reaction-diffusion model with mass action incidences, and France as a case example. Mustafa Turkyilmazoglu in [43] formulated and studied a simplistic reaction-diffusion model to mathematically explore the spatio-temporal development of the concentration of indoor aerosols containing infectious COVID-19 respiratory virus nuclei. Zhu and Zhu in [49] constructed a time delay reaction-diffusion model including relapse, time delay, home quarantine and temporal-spatial heterogeneous environment that affect the spread of COVID-19.

Note that the above mentioned authors do not integrate vaccination in their models. In [4], we formulated and studied a $SQVEAIHR - B$ Covid-19 type compartmental model in which vaccinated individuals are divided into two different groups: the ones who take the first dose and the ones who takes the second dose after taken the first dose. Model formulation was done using both integer and non-integer derivative in the Caputo Sense, with application to German data. In the present study, we formulate and study an SVEAIR type reaction-diffusion model to traduce the Covid-19 transmission dynamics. The proposed model here takes into account the reinfection and the vaccination process with Germany as a case study. One main goal here is to compare quantitatively the model formulated with ordinary differential equations (ODE) and the corresponding reaction-diffusion model with partial differential equation (PDE). Our new contributions are:

1. We first analyse the ODE model by determining the control reproduction number denoted by \mathcal{R}_c and prove the global asymptotic stability of the disease-free equilibrium point (DFEP) whenever $\mathcal{R}_c < 1$. Then, we prove the existence of at least one endemic equilibrium point (EEP) when $\mathcal{R}_c > 1$.
2. We then perform parameter estimation using real data from Germany, as well as sensitivity analysis.
3. After that, we extend the ode model by including the diffusion terms to obtain a reaction-diffusion PDE model. We prove the non-negativity of state variables, as well as the existence and uniqueness of solutions. Asymptotic stability results of the DFEP of the ODE model is extended to obtain the asymptotic stability of the DFEP of the PDE model whenever the control reproduction number \mathcal{R}_c is less than one.
4. Numerical simulations are finally performed by considering:
 - (a) Constant parameters and time-dependent parameters,
 - (b) Two cases:

- i. Initial population is completely susceptible to infection everywhere except for one small region in the very south of Germany, where there are also infected persons;
- ii. When we add a second peak in western Germany, where a major outbreak of Covid-19 occurred in early 2020.

The outline of the work is as follows: the formulation of the ODE compartmental model as well as its theoretical analysis is done in section 2. Section 3 is devoted to model calibration, forecasting and global sensitivity analysis. The reaction-diffusion model is formulated and studied in section 4. Section 5 is devoted to the numerical scheme and simulation results. We end the paper with a conclusion and perspectives.

2 Model formulation

The model we consider here is an extension of an SEIR-type compartmental model, in which we take into account reinfection as well as the vaccination process. The total population at each time t , denoted by $N(t)$, is split into six states or compartments as follows: the susceptible people denoted by $S(t)$, vaccinated people denoted by $V(t)$, infected people in the latent stage denoted by $E(t)$, infected people without symptoms (asymptomatic) denoted by $A(t)$, infected people with symptoms (symptomatic) denoted by $I(t)$, and recovered people denoted by $R(t)$. So, $N(t) = S(t) + V(t) + E(t) + A(t) + I(t) + R(t)$. In this model, the compartment $I(t)$ includes all detected cases as well as hospitalized cases, while $A(t)$ includes all people who are infectious, but not tested and do not present any symptoms of the disease. We consider immigration of vaccinated people into the system. Thus, considering the parameter Λ as the recruitment rate of non-infected people, a rate r_2 of these recruited people is vaccinated while the rest denoted by r_1 is not vaccinated. Among these non-vaccinated people, a rate of c_1 will be vaccinated while among vaccinated people, a rate of c_2 will lose their immunity conferred by the vaccine and become again susceptible. Susceptible people can contract the virus by direct contact with either asymptomatic or symptomatic individuals at the rate $\lambda(t) = \frac{\beta (A(t) + \eta I(t))}{N(t)}$, where β represents the transmission rate, while η represent the modification parameter due to the fact that people who are tested positive are considered as being less infectious because they must take control measures (isolation, quarantine, treatment, ...) to limit the disease transmission. To represent the vaccine efficacy, we introduce the parameter $\phi_1 = (1 - \epsilon)$, where ϵ represents the Covid-19 vaccine efficacy. Thus, the fraction of $\phi_1 \lambda(t)$ will become infected after close contact with an infectious individual. After $1/\gamma$ days which represents the latent period, infected people will become either in the A compartment or the I compartment. Asymptomatic people will move either in the compartment I or the recovered compartment R at the rates $a_2 \sigma$ and $a_1 \sigma$, respectively. Symptomatic people can recover from the infection either naturally or after treatment at a rate θ . In the opposite case, some of them will die of the disease. So, the parameter δ represents the disease-induced death. Recovered people can become reinfected at a rate $\phi_2 \lambda(t)$, where ϕ_2 represents the rate of recovered people who will become infected again. In each compartment, people can die naturally with a natural death rate μ .

The Covid-19 transmission dynamics model expressed using ODEs looks as follows:

$$\left\{ \begin{array}{l} \frac{dS(t)}{dt} = r_1\Lambda + c_2V(t) - \left[\overbrace{c_1 + \mu}^{k_1} + \frac{\overbrace{\beta(A(t) + \eta I(t))}^{\lambda(t)}}{N} \right] S(t), \\ \frac{dV(t)}{dt} = r_2\Lambda + c_1S(t) - \left[\overbrace{\mu + c_2 + \phi_1}^{k_2} \frac{\beta(A(t) + \eta I(t))}{N} \right] V(t), \\ \frac{dE(t)}{dt} = \frac{\beta(A(t) + \eta I(t))}{N} (S(t) + \phi_1V(t) + \phi_2R(t)) - \overbrace{(\mu + \gamma)}^{k_3} E(t), \\ \frac{dA(t)}{dt} = p\gamma E(t) - \overbrace{(\mu + \sigma)}^{k_4} A(t), \\ \frac{dI(t)}{dt} = q\gamma E(t) + a_2\sigma A(t) - \overbrace{(\mu + \delta + \theta)}^{k_5} I(t), \\ \frac{dR(t)}{dt} = a_1\sigma A(t) + \theta I(t) - \left[\mu + \phi_2 \frac{\beta(A(t) + \eta I(t))}{N} \right] R(t) \end{array} \right. \quad (1)$$

with $r_1 + r_2 = 1$, $p + q = 1$, and $a_1 + a_2 = 1$.

Remark 1. *It is important to note that model described by the system (1) is a compact form of the model studied in [4]. Indeed, in [4], the proposed Covid-19 model included two vaccine dose compared to the present model (1). In addition, the (1) model does not take into account people in quarantine, people in hospitals, and viruses in the environment.*

Setting $X = (S, V, E, A, I, R)'$ the vector of state variables and $\Pi = \{X \in \mathbb{R}^6 : X \geq \mathbf{0}_{\mathbb{R}^6}\}$, system (1) can be write in the following compact form

$$\left\{ \begin{array}{l} \frac{dX}{dt} = \mathcal{F}(t, X) = (\mathcal{F}_1(X), \mathcal{F}_2(X), \dots, \mathcal{F}_6(X))', \\ X(t_0) = X_0 = (S_0, V_0, E_0, A_0, I_0, R_0)' \geq \mathbf{0}_{\mathbb{R}^6}, \end{array} \right. \quad (2)$$

where $\mathcal{F} : \mathbb{R}^6 \rightarrow \mathbb{R}^6$ is a continuously differentiable function on \mathbb{R}^6 , and $(\bullet)'$ stands for the transposition operator. According to [45, Theorem III.10.VI], for $X(0) \in \Pi$, a unique solution of (1) exists, at least locally, and remains in Π for its maximal interval of existence [45, Theorem III.10.XVI]. Hence model (1) is biologically well-defined.

Model (1) is defined in the following set

$$\mathbf{W} = \left\{ (S, V, E, A, I, R)' \in \mathbb{R}_+^6 : 0 < N := S + V + E + A + I + R \leq \frac{\Lambda}{\mu} \right\},$$

which is invariant for the system (1).

The above statement is obtained in the same way as the results obtained in [4, Theorem 2].

2.1 The disease-free equilibrium and the basic reproduction number

In the absence of disease, i.e. for $A = I = B = 0$, model (1) always admits the equilibrium $\mathcal{E}_0 = (S_0, V_0, 0, 0, 0, 0)'$ called the disease-free equilibrium, with $S_0 = \frac{(c_2r_2 + r_1k_2)\Lambda}{k_1k_2 - c_1c_2}$ and $V_0 = \frac{(k_1r_2 + c_1r_1)\Lambda}{k_1k_2 - c_1c_2}$. Note that $k_1k_2 - c_1c_2 = \mu^2 + (c_2 + c_1)\mu > 0$, and $S_0 + V_0 = N_0 = \frac{\Lambda}{\mu}$.

To compute the control reproduction number, denoted by \mathcal{R}_c , we will use the next generation approach (see [11, 44]). Let us set $y = (E, A, I)'$. The vector \mathcal{Z} and \mathcal{W} for the new infection terms and the remaining transfer terms for y are, respectively, given by

$$\mathcal{Z} = \begin{pmatrix} \frac{\beta(A(t) + \eta I(t))}{N} (S + \phi_1 V + \phi_2 R) \\ 0 \\ 0 \end{pmatrix},$$

and

$$\mathcal{W} = \begin{pmatrix} k_3 E \\ -p\gamma E + k_4 A, \\ -q\gamma E - a_2 \sigma A + k_5 I, \end{pmatrix}.$$

Their Jacobian matrices evaluated at \mathcal{E}_0 are respectively given by

$$Z = \begin{pmatrix} 0 & \beta \frac{N_1}{N_0} & \beta \eta \frac{N_1}{N_0} \\ 0 & 0 & 0 \\ 0 & 0 & 0 \end{pmatrix} \text{ and } W = \begin{pmatrix} k_3 & 0 & 0 \\ -p\gamma & k_4 & 0 \\ -q\gamma & -a_2 \sigma & k_5 \end{pmatrix}, \quad (3)$$

with $N_1 = S_0 + \phi_1 V_0$. Then, the control reproduction number \mathcal{R}_c is defined, following [11, 44], as the spectral radius of the next generation matrix, ZW^{-1} where

$$ZW^{-1} = \begin{pmatrix} \frac{N_1 \beta \eta (a_2 p \sigma \gamma + k_4 q \gamma)}{N_0 k_3 k_4 k_5} + \frac{N_1 \beta p \gamma}{N_0 k_3 k_4} & \frac{N_1 a_2 \beta \eta \sigma}{N_0 k_4 k_5} + \frac{N_1 \beta}{N_0 k_4} & \frac{N_1 \beta \eta}{N_0 k_5} \\ 0 & 0 & 0 \\ 0 & 0 & 0 \end{pmatrix}.$$

Therefore, the control reproduction number, \mathcal{R}_c , is the sum of two main contributions, namely, humans and environment, as follows:

$$\mathcal{R}_c := \rho(ZW^{-1}) = \frac{N_1 \beta \eta \gamma (a_2 p \sigma + k_4 q)}{N_0 k_3 k_4 k_5} + \frac{N_1 \beta p \gamma}{N_0 k_3 k_4}, \quad (4)$$

where $\rho(\bullet)$ represents the spectral radius operator.

From [44, Theorem 2], we have the following result.

Lemma 1. (Local stability of the DFE) *The stationary point \mathcal{E}_0 of system (1) is locally asymptotically stable (LAS) if $\mathcal{R}_c < 1$, and unstable otherwise.*

We also have the following result:

Theorem 1. *The disease-free equilibrium \mathcal{E}_0 is globally asymptotically stable in \mathbf{W} whenever $\mathcal{R}_c < 1$.*

Proof. Considering only the infected compartments of system (1), we obtain

$$\begin{pmatrix} \frac{dE}{dt} \\ \frac{dA}{dt} \\ \frac{dI}{dt} \end{pmatrix} = (Z - W) \begin{pmatrix} E(t) \\ A(t) \\ I(t) \end{pmatrix} - \mathcal{M}(S, V, E, A, I, R), \quad (5)$$

where Z and W are the same matrices used to compute the control reproduction number (see Eq. (4)), and

$$\mathcal{M}(S, V, E, A, I, R) = \begin{pmatrix} \beta(A + \eta I) \left(\frac{N_1}{N_0} - \frac{(S + \phi_1 V + \phi_2 R)}{N} \right) \\ 0 \\ 0 \end{pmatrix}.$$

If $\frac{N_1}{N_0} - \frac{(S + \phi_1 V + \phi_2 R)}{N} \geq 0$ in \mathcal{W} , then, it follows that $\mathcal{M}(S, V, E, A, I, R) \geq \mathbf{0}_{\mathbb{R}^3}$. This means that

$$\begin{pmatrix} \frac{dE}{dt} \\ \frac{dA}{dt} \\ \frac{dI}{dt} \end{pmatrix} \leq (Z - W) \begin{pmatrix} E(t) \\ A(t) \\ I(t) \end{pmatrix}.$$

Note that

$$W^{-1} = \begin{pmatrix} \frac{1}{k_3} & 0 & 0 \\ \frac{p\gamma}{k_3 k_4} & \frac{1}{k_4} & 0 \\ \frac{a_2 p \sigma \gamma + k_4 q \gamma}{k_3 k_4 k_5} & \frac{a_2 \sigma}{k_4 k_5} & \frac{1}{k_5} \end{pmatrix} \geq \mathbf{0}_{\mathbb{R}^{3 \times 3}}$$

We also have, from (3), $Z \geq 0$. Thus, from [39, Theorem 2.1], there exists a Lyapunov function for system (1) expressed as $\mathcal{Q}(S, V, E, A, I, R) = w' W^{-1}(E, A, I)'$ where w' is the left eigenvector of the nonnegative matrix $W^{-1}Z$ corresponding to the eigenvalue \mathcal{R}_c . This implies that if $\mathcal{R}_c < 1$,

$$\frac{d\mathcal{Q}}{dt} = (\mathcal{R}_c - 1) w'(E, A, I) - w' W^{-1} \mathcal{M}(S, V, E, A, I, R) \leq 0$$

whenever the condition $\frac{N_1}{N_0} - \frac{(S + \phi_1 V + \phi_2 R)}{N} \geq 0$ holds. It follows from the LaSalle invariance principle [27] that every solution of (1) with initial conditions in \mathbf{W} converges to the DFE \mathcal{E}_0 when $t \rightarrow +\infty$. That is $(E, A, I) \rightarrow (0, 0, 0)$, $S \rightarrow S_0$ and $V \rightarrow V_0$ when $t \rightarrow +\infty$, which is equivalent to $(S, V, E, A, I, R) \rightarrow (S_0, V_0, 0, 0, 0, 0)$ when $t \rightarrow +\infty$. Thus, by the LaSalle invariance principle [27], the disease-free equilibrium \mathcal{E}_0 is globally asymptotically stable in \mathbf{W} whenever $\mathcal{R}_c < 1$. This ends the proof of Theorem 1. \square

2.2 Existence of the endemic equilibrium and its stability

Let $\mathcal{E} = (S^*, V^*, E^*, A^*, I^*, R^*)'$ be an equilibrium point of model (1) obtained by setting the right hand-side of (1) equal to zero, that is

$$\begin{cases} r_1 \Lambda + c_2 V^* - k_1 S^* - \lambda^* S^* & = 0, \\ r_2 \Lambda + c_1 S^* - [k_2 + \phi_1 \lambda^*] V^* & = 0, \\ \lambda^* (S^* + \phi_1 V^* + \phi_2 R^*) - k_3 E^* & = 0, \\ p\gamma E^* - k_4 A^* & = 0, \\ q\gamma E^* + a_2 \sigma A^* - k_5 I^* & = 0, \\ a_1 \sigma A^* + \theta I^* - [\mu + \phi_2 \lambda^*] R^* & = 0. \end{cases} \quad (6)$$

Solving the above system gives

$$\left\{ \begin{array}{l} S^* = \frac{r_1 \Lambda \phi_1 \lambda^* + \overbrace{(c_2 r_2 + r_1 k_2)}^{k_7} \Lambda}{\lambda^* (\phi_1 \lambda^* + k_2) + k_1 \phi_1 \lambda^* + \overbrace{k_1 k_2 - c_1 c_2}^{k_6}} = \frac{r_1 \Lambda \phi_1 \lambda^* + k_7 \Lambda}{\lambda^* (\phi_1 \lambda^* + k_2) + k_1 \phi_1 \lambda^* + k_6}, \\ V^* = \frac{r_2 \Lambda + c_1 S^*}{[k_2 + \phi_1 \lambda^*]}, E^* = \frac{\lambda^* (S^* + \phi_1 V^* + \phi_2 R^*)}{k_3}, A^* = \frac{p \gamma E^*}{k_4}, \\ I^* = \frac{q \gamma E^* + a_2 \sigma A^*}{k_5}, R^* = \frac{a_1 \sigma A^* + \theta I^*}{[\mu + \phi_2 \lambda^*]}, N^* = \frac{\Lambda - \delta I^*}{\mu}, \end{array} \right. \quad (7)$$

where $\lambda^* := \beta \frac{(A^* + \eta I^*)}{N^*}$ is any nonnegative solutions of the following equation

$$\lambda^* [\mathcal{A}_3(\lambda^*)^3 + \mathcal{A}_2(\lambda^*)^2 + \mathcal{A}_1 \lambda^* + \mathcal{A}_0] = 0, \quad (8)$$

where

$$\begin{aligned} \mathcal{A}_3 &= -\phi_1 \phi_2 (r_1 \mu (1 - \phi_1) + \phi_1 (\mu + c_1) + c_2) (a_2 \eta p \sigma + k_4 \eta q + k_5 p) \\ &\quad \times [(\theta - \delta) (a_2 p \sigma \gamma + k_4 q \gamma) + k_5 \mu (\mu + k_2) + k_5 \gamma \sigma (1 - a_1 p)], \\ \mathcal{A}_0 &= k_3 k_4 k_5 \mu^2 (\mu + c_2 + c_1) (r_1 \mu (1 - \phi_1) + \phi_1 (\mu + c_1) + c_2) (a_2 \eta p \sigma + k_4 \eta q + k_5 p) (\mathcal{R}_c - 1). \end{aligned}$$

Assume that $\theta_1 > \delta$. Since $a_1 + a_2 = 1$ and $p + q = 1$, it follows that $1 - a_1 p > 0$. Thus the coefficient \mathcal{A}_3 is always negative. Coefficient \mathcal{A}_0 is negative (resp. positive) if and only if $\mathcal{R}_c < 1$ (resp. $\mathcal{R}_c > 1$). Using the Descartes rule of signs, we claim the following:

Proposition 1.

1. If $\mathcal{R}_c > 1$, then model (1) admits:

- (i) exactly one endemic equilibrium point if and only if $(\mathcal{A}_2 > 0 \ \& \ \mathcal{A}_1 > 0)$ or $(\mathcal{A}_2 < 0 \ \& \ \mathcal{A}_1 > 0)$ or $(\mathcal{A}_2 < 0 \ \& \ \mathcal{A}_1 < 0)$;
- (ii) exactly three endemic equilibrium points if and only if $(\mathcal{A}_2 > 0 \ \& \ \mathcal{A}_1 < 0)$;

2. If $\mathcal{R}_c < 1$, then model (1) admits:

- (iii) exactly two endemic equilibrium points if and only if $(\mathcal{A}_2 > 0 \ \& \ \mathcal{A}_1 > 0)$ or $(\mathcal{A}_2 > 0 \ \& \ \mathcal{A}_1 < 0)$ or $(\mathcal{A}_2 < 0 \ \& \ \mathcal{A}_1 > 0)$;
- (iv) Otherwise no endemic equilibrium exists.

Item (iii) of the above Proposition suggests the possibility of occurrence of the backward bifurcation phenomenon [3] in model (1), i.e when the disease-free equilibrium point co-exists with two endemic equilibrium points (one is locally stable and the other is unstable) whenever the biological threshold \mathcal{R}_c is less than one. Thanks to Theorem 1, we conclude that even if the disease-free equilibrium co-exists with two endemic equilibrium points when $\mathcal{R}_c < 1$, these last ones are either always unstable or do not belong to the set \mathbf{W} .

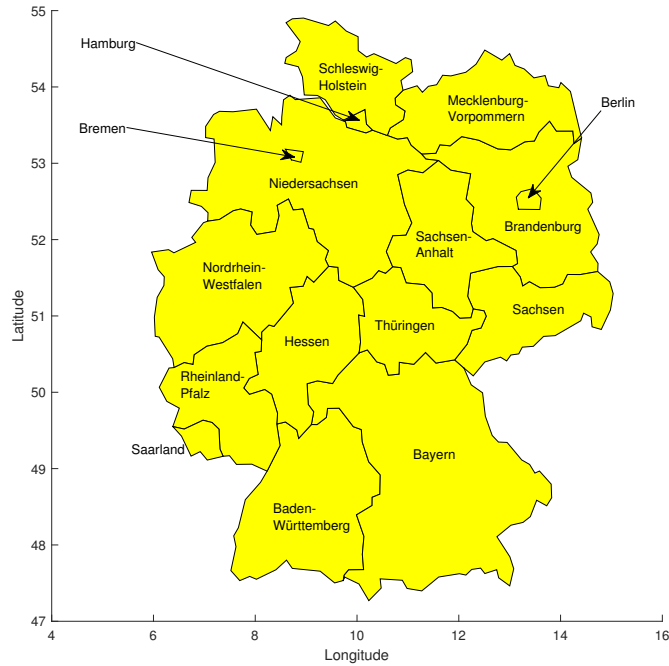


Figure 1: Map of the Federal Republic of Germany with its sixteen states.

3 Model calibration, forecasting, and sensitivity analysis

3.1 Model calibration and forecasting

The start date of mass vaccination in Germany was Sunday, 27 December 2020 [16]. Since then, several constraint measures were taken to ensure that the majority of inhabitants is vaccinated. We consider the daily infected reported cases in Germany from December 31, 2020, to February 28, 2021 [20]. The map of the Federal Republic of Germany is depicted in Figure 1.

In model (1), there are eighteen parameters. Of these, seven parameters are either estimated or taken from the existing literature, while the other remaining parameters must be calibrated using data. Taking the total approximate population of Germany in 2021 equal to $N(0) = 83,900,473$ [17, 28], the recruitment rate is equal to $\Lambda = \mu N(0)$. The initial conditions subject to data fitting are: $S(0) = 83674478$, $V(0) = 49939$, $E(0) = 22924$, $A(0) = 22920$, $I(0) = 32552$, and $R(0) = 97660$. The nonlinear square method is used to fit the model to the real data. It provides realistic values of model parameters, which is beneficial when we want to forecast the evolution of the disease in a given time interval. We perform experiments until the desired accurate fitting of the model is achieved. After numerically solving the optimization problem

$$\min_{\Gamma} \| I_{\text{predict}} - I_{\text{data}} \|, \quad (9)$$

where $\Gamma = \{\beta, \phi_2, r_1, a_1, c_2, \eta, \theta, \gamma, \}$, we obtain the results in Table 1. The model simulation versus data fitting is shown in Figure 2. The value of the cumulative control reproduction number computed with the parameter values in Table 1 is $\mathcal{R}_c = 1.127472860225384$.

The prediction (forecasting) of the Covid-19 situation is depicted on Figure 3. It is clear that, even if the total number of detected cases is decreasing, it is clear that the Covid-19 pandemic will still be relevant and will remain a public health problem for the next years.

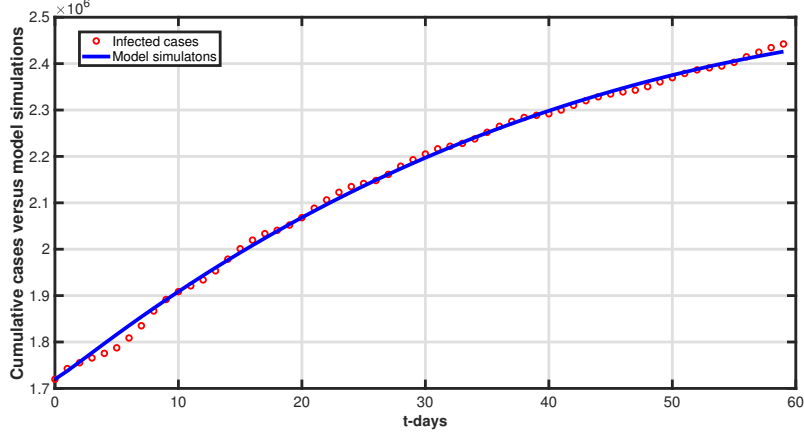


Figure 2: Cumulative reported cases in Germany versus model fitting. $t = 0$ stands for December 31, 2020 and $t = 59$ stands for February 28, 2021.

Table 1: Model parameters and their estimated values.

Parameter	Value/per day	Source	Parameter	Value/per day	Source
Λ	$N(0) \times \mu$	Estimated, [28]	σ	0.1428	[41]
μ	$\frac{1}{81.72 \times 365}$	[28]	ϕ_1	0.52	[14]
β	0.924293447982239	Fitted	c_1	0.77	[35]
ϕ_2	0.000626319868356	Fitted	δ	0.0018	[32]
r_1	0.025344642995677	Fitted	r_2	$1 - r_1$	From Eq.(1)
a_1	0.349489753971447	Fitted	a_2	$1 - a_1$	From Eq.(1)
c_2	0.185640604312541	Fitted	θ	0.557147574601118	Fitted
η	0.356255781186421	Fitted	γ	0.017296258650737	Fitted
p	0.2	Assumed	q	$1 - p$	From Eq.(1)

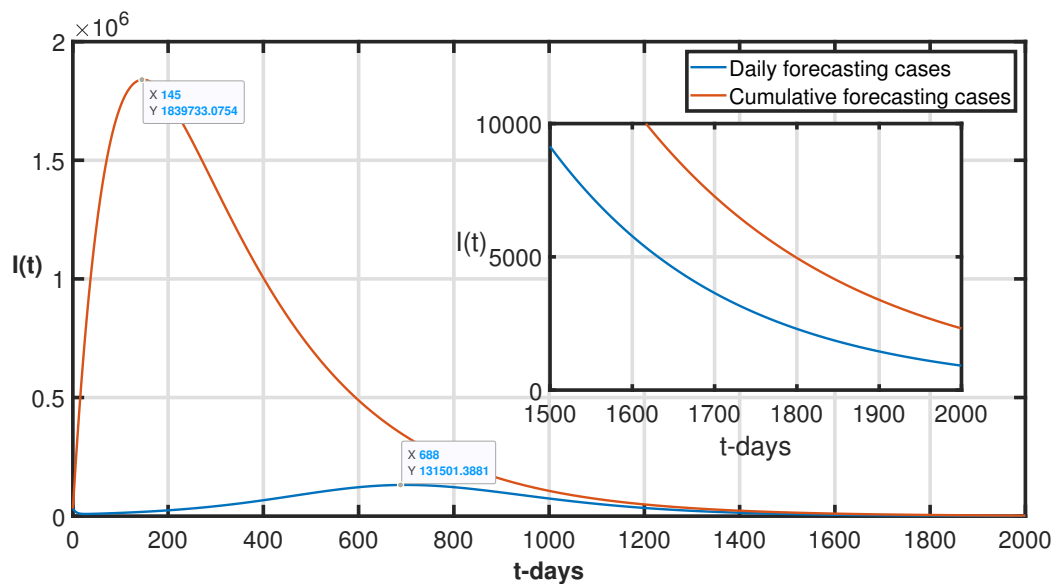
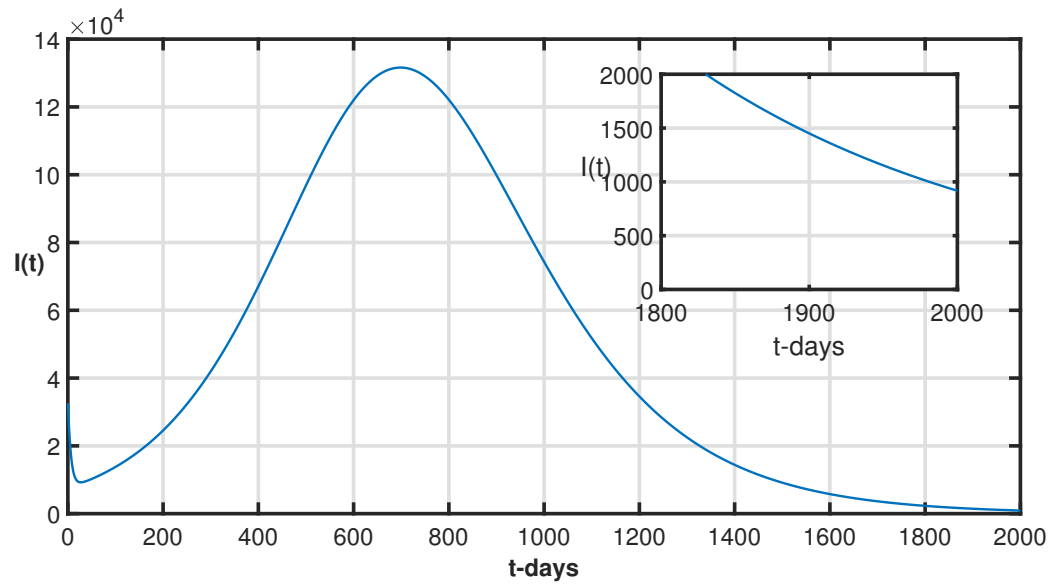


Figure 3: Long-term Covid-19 prediction.

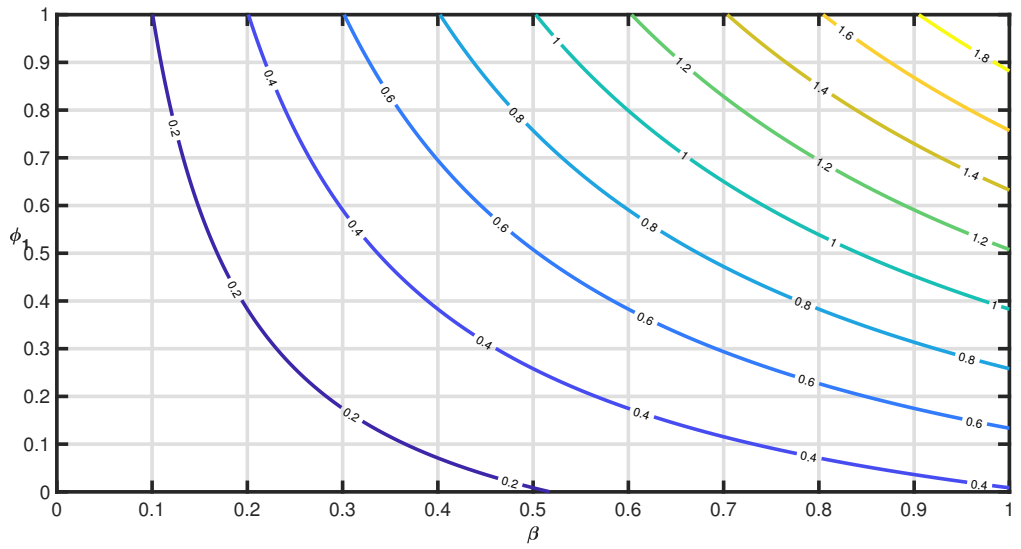
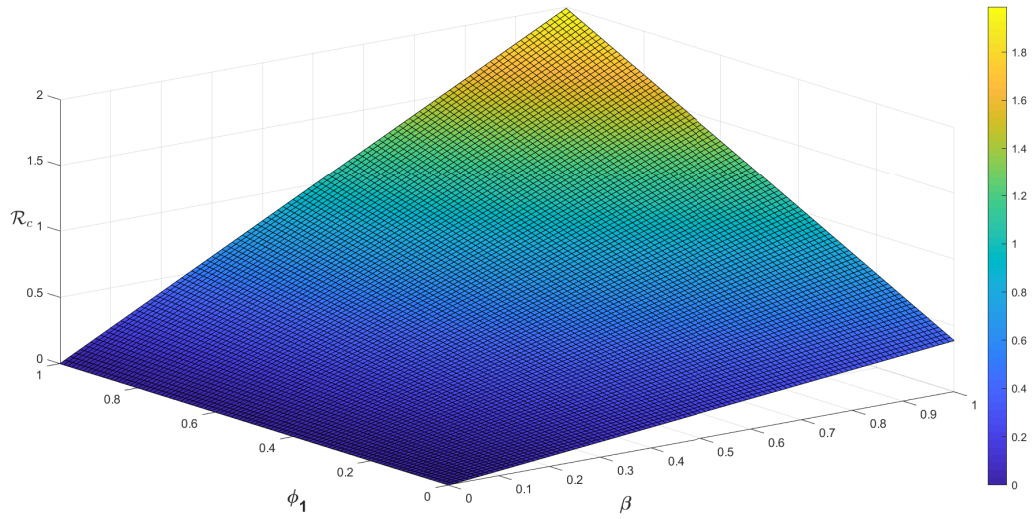
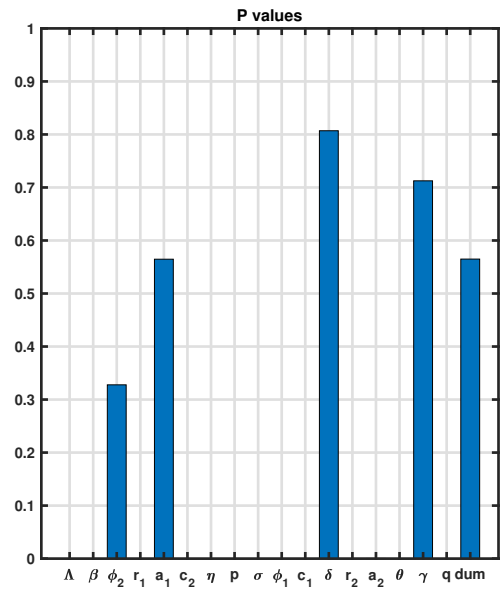
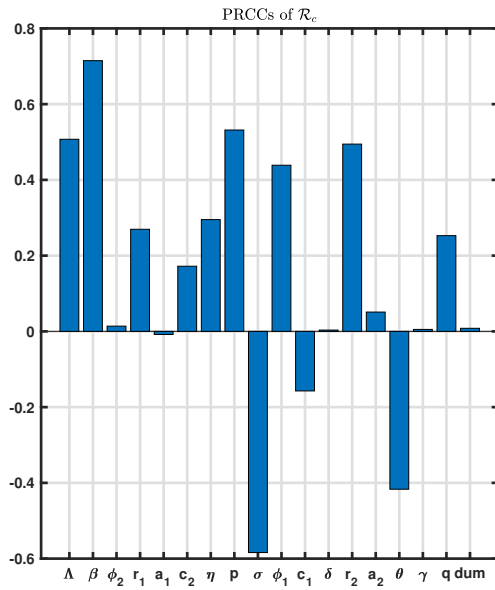


Figure 4: The control reproduction number in term of β and ϕ_1 .

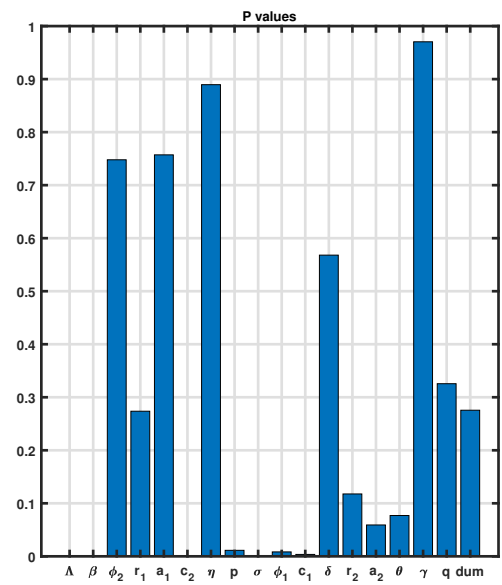
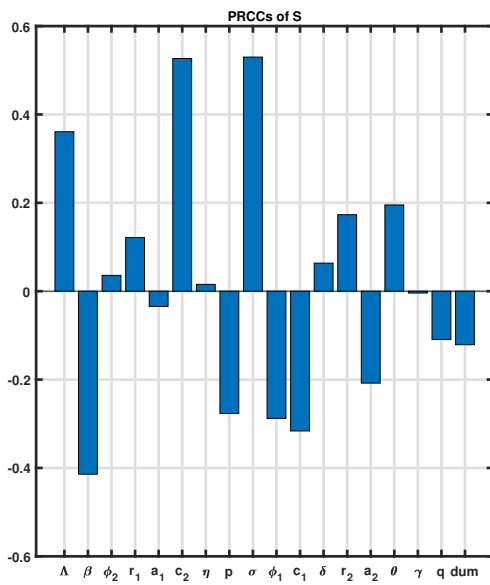
3.2 Sensitivity analysis

To measure the correlation between the model's parameters and the control reproduction number \mathcal{R}_c , as well as the state variables of (1), we perform a global sensitivity analysis by computing the partial rank correlation coefficient (PRCC) between \mathcal{R}_c (respectively the state variables) and model parameters. These are used to measure the nonlinear (but monotonic) relationship between model parameters and model outputs, cf. [12, 30, 47]. The sampling technique used here is the Latin Hypercube Sampling (LHS). The number of runs is equal to 5000, and each model parameter is supposed uniformly distributed with its mean value listed in Table 1.

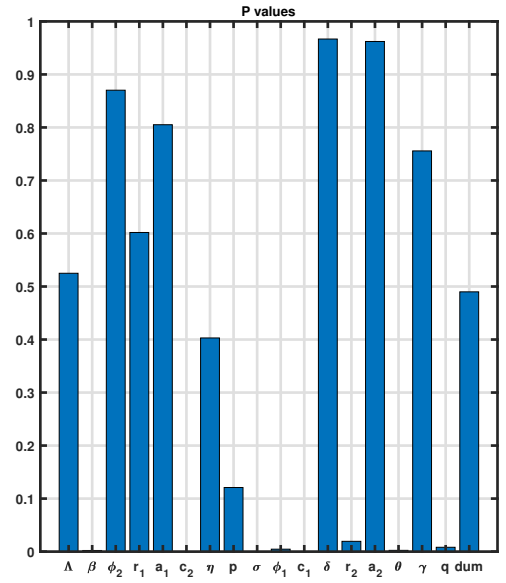
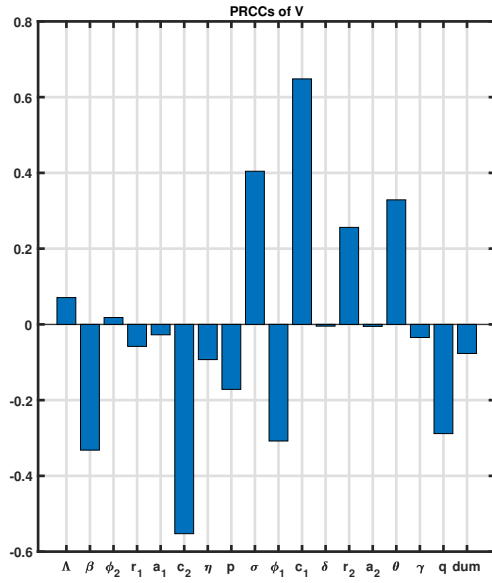
PRCCs between \mathcal{R}_c (respectively state variables) and model parameters are depicted in Figure 8. The most influential parameters are those whose absolute PRCCs are greater than -0.5 [47] with a p-value less than 0.001.



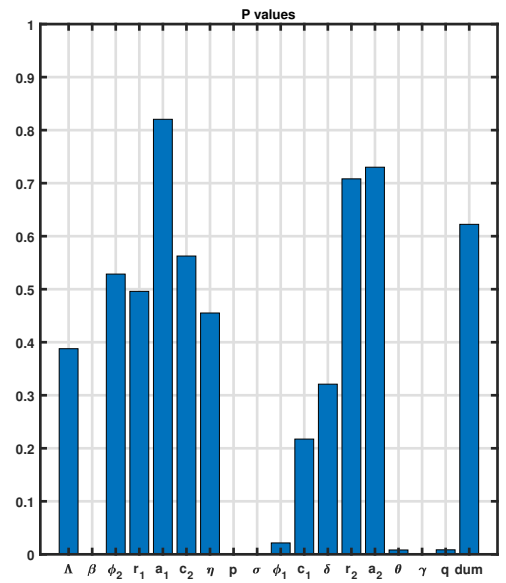
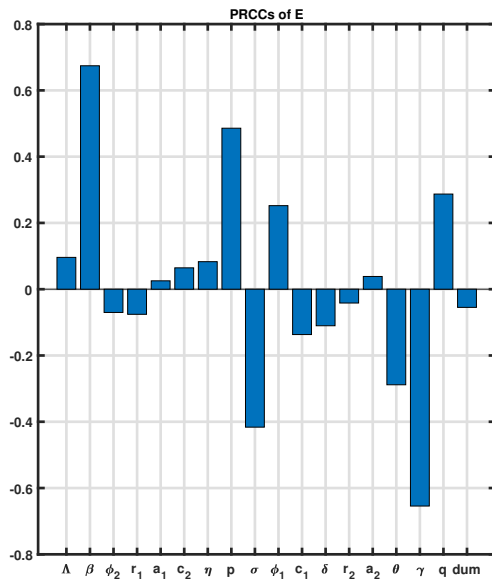
(a) PRCCs between \mathcal{R}_c and model parameters



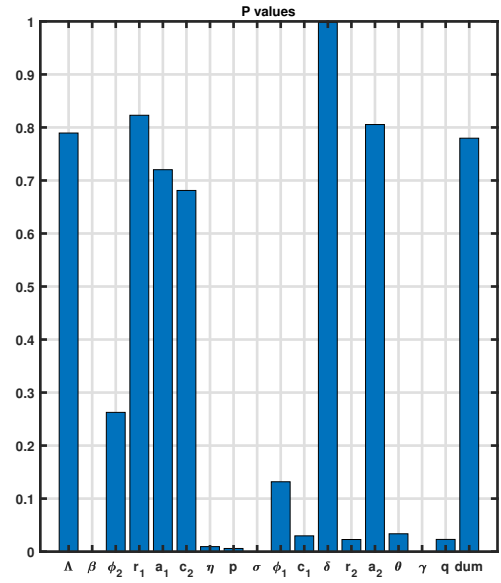
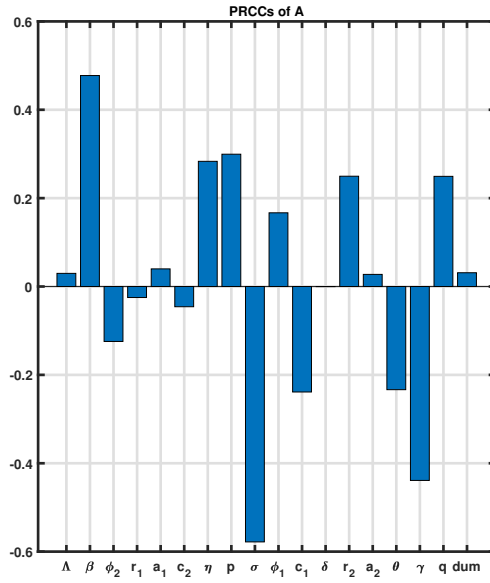
(b) PRCCs between S and model parameters



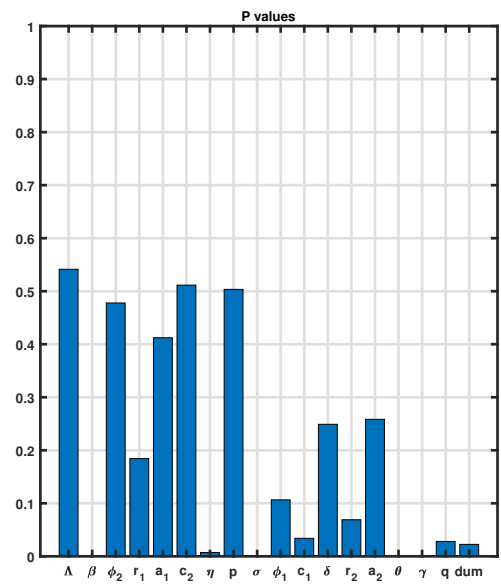
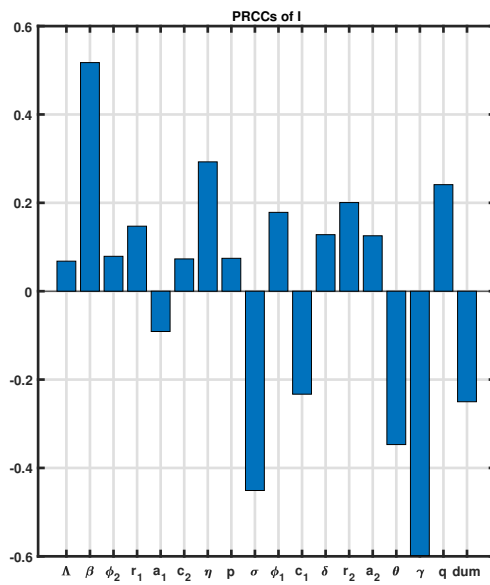
(a) PRCCs between V and model parameters



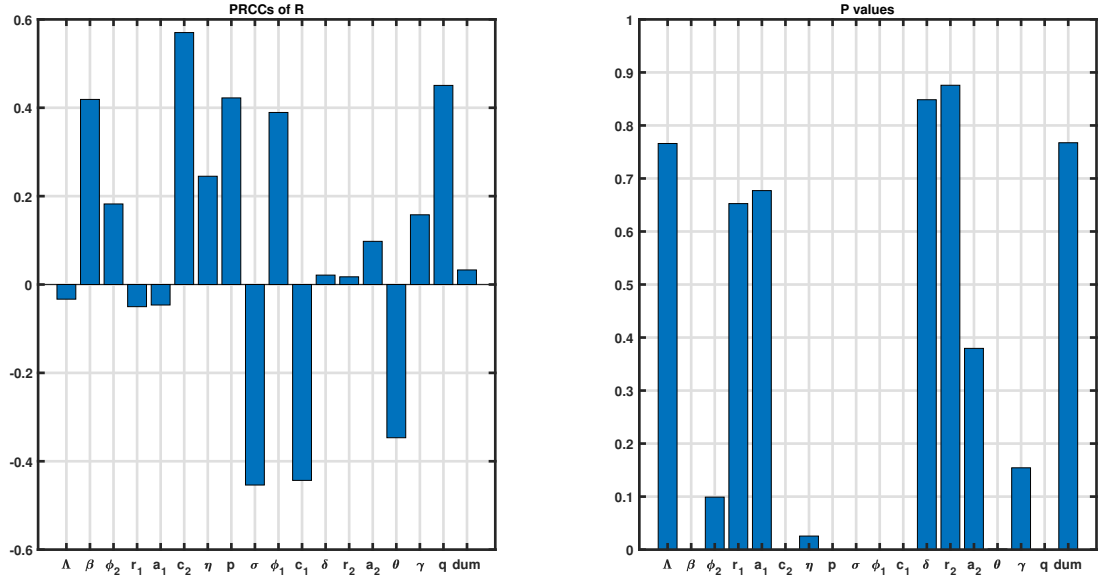
(b) PRCCs between E and model parameters



(a) PRCCs between A and model parameters



(b) PRCCs between I and model parameters



(a) PRCCs between R and model parameters

Figure 8: Partial Rank Corellation coefficients between \mathcal{R}_c and (a) model parameters, and (b)-(g) state variables. "dum" is for the dummy parameter.

From figure 8 (panel (a)), it follows that the parameters β , σ , Λ and p are the parameters most correlated to the control reproduction number \mathcal{R}_c . This suggests that intensification of some control strategies like individual protection (hand washing, wearing a mask), effective treatment, quarantine, and confinement can lead to a decrease in the control reproduction number. From panels (b)-(f) of figure 8, it follows that β , σ , Λ , γ and p are the most important parameters of the model (1). This suggests that all actions which can contribute to reducing contact between infected people and healthy individuals (wearing masks, social distancing, quarantine and/or confinement) as well as their identification (massive tests) and treatment, over a long period of time, could permit to reduce the disease spread in the population.

4 Reaction-diffusion model and its analysis

Now, we extend the ODE model (1) by introducing a diffusion process to obtain a reaction-diffusion model. State variables thus are time and space-dependent. The Covid-19 reaction-

diffusion model is then given as follows:

$$\left\{ \begin{array}{l} \frac{\partial S(x,t)}{\partial t} - \kappa_s \Delta S(x,t) = r_1 \Lambda + c_2 V(x,t) - \left[k_1 + \frac{\beta (A(x,t) + \eta I(x,t))}{N(t)} \right] S(x,t), \quad x \in \Sigma \\ \frac{\partial V(x,t)}{\partial t} - \kappa_v \Delta V(x,t) = r_2 \Lambda + c_1 S(x,t) - \left[k_2 + \phi_1 \frac{\beta (A(x,t) + \eta I(x,t))}{N(t)} \right] V(x,t), \quad x \in \Sigma \\ \frac{\partial E(x,t)}{\partial t} - \kappa_e \Delta E(x,t) = \frac{\beta [A(x,t) + \eta I(x,t)] (S(x,t) + \phi_1 V(x,t) + \phi_2 R(x,t))}{N(t)} - k_3 E(x,t), \quad x \in \Sigma \\ \frac{\partial A(x,t)}{\partial t} - \kappa_a \Delta A(x,t) = p\gamma E(x,t) - k_4 A(x,t), \quad x \in \Sigma \\ \frac{\partial I(x,t)}{\partial t} - \kappa_i \Delta I(x,t) = q\gamma E(x,t) + a_2 \sigma A(x,t) - k_5 I(x,t), \quad x \in \Sigma \\ \frac{\partial R(x,t)}{\partial t} - \kappa_r \Delta R(x,t) = a_1 \sigma A(x,t) + \theta I(x,t) - \left[\mu + \phi_2 \frac{\beta (A(x,t) + \eta I(x,t))}{N(t)} \right] R(x,t), \quad x \in \Sigma \\ \frac{\partial S(x,t)}{\partial \phi} = \frac{\partial V(x,t)}{\partial \phi} = \frac{\partial E(x,t)}{\partial \phi} = \frac{\partial A(x,t)}{\partial \phi} = \frac{\partial I(x,t)}{\partial \phi} = \frac{\partial R(x,t)}{\partial \phi} = 0, \quad x \in \partial \Sigma \end{array} \right. \quad (10)$$

with the following initial conditions

$$\left\{ \begin{array}{l} S(x,0) = S_0(x) > 0, V(x,0) = V_0(x) \geq 0, E(x,0) = E_0(x) \geq 0, \\ A(x,0) = A_0(x) \geq 0, I(x,0) = I_0(x) \geq 0, R(x,0) = R_0(x) \geq 0. \end{array} \quad x \in \Sigma. \quad (11)$$

In system (10), t denotes a nonnegative time; Σ denotes a bounded domain of \mathbb{R}^m ($m \geq 1$) with smooth boundary $\partial \Sigma$, ϕ is the outward normal to $\partial \Sigma$; $\kappa_s > 0$, $\kappa_v > 0$, $\kappa_e > 0$, $\kappa_a > 0$, $\kappa_i > 0$, $\kappa_r > 0$ are the diffusion rates; $X_j(x,t)$, $j \in \{1, 2, \dots, 6\}$, denote the number of population in the compartment X_j in position x at time t , with $X(x,t) = (S(x,t), V(x,t), E(x,t), A(x,t), I(x,t), R(x,t))$.

Note that in the first open quadrant, the function $f(X) = S(A + \eta I)/N$ is continuous Lipschitz for each X_j , $j \in \{1, 2, \dots, 6\}$, with $X = (S, V, E, A, I, R)$. Thus, we can extend its definition to the entire first quadrant by setting $f(0, X_I) = f(X_S, 0) = 0$, where $X_S = (S, V, R)$ and $X_I = (E, A, I)$.

4.1 Qualitative analysis of the model

We examine the basic features of the Initial Bounded Value Problem (IVBP) (10)-(11). Since the model deals with humans population, all its state variables should be positive for all $t > 0$. In what follows, we thus establish the existence, uniqueness, positivity, and boundedness of the solution of the model (10)-(11).

Theorem 2. *For any given initial conditions which satisfy (11), the solution of model (10)-(11) is nonnegative, unique and bounded in $[0, \infty)$.*

Proof. The IVBP model (10)-(11) can be rewritten in the Banach space $\mathcal{B} = C(\overline{\Sigma})$ as follows:

$$\left\{ \begin{array}{l} \frac{dX(t)}{dt} = \mathbf{A}X(t) + \mathbf{f}(X(t)), \quad t > 0 \\ X(0) = X_0 \geq \mathbf{0}_{\mathbb{R}^6}, \end{array} \right. \quad (12)$$

where $X = (S, V, E, A, I, R)'$, $X_0 = (S_0(x), V_0(x), E_0(x), A_0(x), I_0(x), R_0(x))'$, and formally

$\mathbf{A}X = (\kappa_s \Delta S, \kappa_v \Delta V, \kappa_e \Delta E, \kappa_a \Delta A, \kappa_i \Delta I, \kappa_r \Delta R)'$, and $\mathbf{f} = (\mathbf{f}_1, \mathbf{f}_2, \mathbf{f}_3, \mathbf{f}_4, \mathbf{f}_5, \mathbf{f}_6)'$, with

$$\left\{ \begin{array}{l} \mathbf{f}_1(X) = r_1 \Lambda + c_2 V(x, t) - \left[k_1 + \frac{\beta (A(x, t) + \eta I(x, t))}{N(t)} \right] S(x, t), \\ \mathbf{f}_2(X) = r_2 \Lambda + c_1 S(x, t) - \left[k_2 + \phi_1 \frac{\beta (A(x, t) + \eta I(x, t))}{N(t)} \right] V(x, t), \\ \mathbf{f}_3(X) = \frac{\beta [A(x, t) + \eta I(x, t)] (S(x, t) + \phi_1 V(x, t) + \phi_2 R(x, t))}{N(t)} - k_3 E(x, t), \\ \mathbf{f}_4(X) = p\gamma E(x, t) - k_4 A(x, t), \\ \mathbf{f}_5(X) = q\gamma E(x, t) + a_2 \sigma A(x, t) - k_5 I(x, t), \\ \mathbf{f}_6(X) = a_1 \sigma A(x, t) + \theta I(x, t) - \left[\mu + \phi_2 \frac{\beta (A(x, t) + \eta I(x, t))}{N(t)} \right] R(x, t). \end{array} \right.$$

\mathbf{f} is locally Lipschitz in \mathcal{B} . For the existence of a local smooth solution see [8, Theorem B.17] or [31, 40]. The positivity follows from [40, Theorem 14.14]

To prove the boundedness of states variables, we will follow [19, Proposition 2.1]. Setting $N(x, t) = S(x, t) + V(x, t) + E(x, t) + A(x, t) + I(x, t) + R(x, t)$, we obtain

$$\begin{aligned} & \frac{\partial N(x, t)}{\partial t} - \kappa_s \Delta S(x, t) - \kappa_v \Delta V(x, t) - \kappa_e \Delta E(x, t) - \kappa_a \Delta A(x, t) - \kappa_i \Delta I(x, t) - \kappa_r \Delta R(x, t) \\ &= \Lambda - \mu N(x, t) - \delta I(x, t), \quad x \in \Sigma, \quad t > 0. \end{aligned}$$

Integrating the above equation over Σ , and using the Neumann boundary condition, we obtain for $t > 0$

$$\begin{aligned} \frac{d}{dt} \int_{\Sigma} N(x, t) dx &= \Lambda \int_{\Sigma} dx - \mu \int_{\Sigma} N(x, t) dx - \delta \int_{\Sigma} I(x, t) dx \\ &\leq \Lambda |\Sigma| - \mu \int_{\Sigma} N(x, t) dx \end{aligned}$$

Integrating the above inequality from 0 and $t > 0$ yields

$$\int_{\Sigma} N(x, t) dx \leq \exp(-\mu t) \int_{\Sigma} N_0 dx + \frac{\Lambda |\Sigma|}{\mu} [1 - \exp(-\mu t)] \quad (13)$$

This implies for $j = 1, 2, \dots, 6$ that

$$\int_{\Sigma} X_j(x, t) dx \leq \int_{\Sigma} N_0 dx + \frac{\Lambda |\Sigma|}{\mu},$$

where $X(x, t) = (S(x, t), V(x, t), E(x, t), A(x, t), I(x, t), R(x, t))$. Thus applying [13, Theorem 1] with $\sigma = p_0 = 1$ to the compact system (2), we conclude that there exists a positive constant \mathcal{M}_1 depending on initial data such that the solution $X = (S, V, E, A, I, R)$ of (2) satisfies

$$\sum_{j=1}^6 \|X_j(\cdot, t)\|_{L^\infty(\Sigma)} \leq \mathcal{M}_1, \quad \forall t \geq 0. \quad (14)$$

Note that (13) implies

$$\lim_{t \rightarrow \infty} \int_{\Sigma} N(x, t) dx \leq \frac{\Lambda |\Sigma|}{\mu}$$

which implies that

$$\lim_{t \rightarrow \infty} \int_{\Sigma} X_j(x, t) dx \leq \frac{\Lambda |\Sigma|}{\mu}, \quad j = 1, 2, \dots, 6.$$

Applying again [37, Lemma 3.1], we can claim that here exists a positive constant \mathcal{M}_2 which does not depend on initial data X_j^0 , $j = 1, 2, \dots, 6$ such that

$$\sum_{j=1}^6 \|X_j(\cdot, t)\|_{L^\infty(\Sigma)} \leq \mathcal{M}_2, \quad \forall t \geq T \quad (15)$$

for some large $T > 0$. This proves that each variable state of PDE model is bounded and hence, the solution exists globally, cf. [8]. This ends the proof. \square

From Theorem 2, it follows that the following set

$$\mathbf{W} = \left\{ (S, V, E, A, I, R) \in \mathbb{R}_+^6 : 0 < N := S + V + E + A + I + R \leq \frac{\Lambda |\Sigma|}{\mu} \right\}$$

is positively invariant for system (10), and the IBVP (10)-(11) defines a dynamical system in it.

4.2 Basic reproduction number and equilibrium points

4.2.1 The basic reproduction number

As for the ODE Covid-19 model (1), the PDE model (10) always has the disease-free equilibrium $\mathcal{E}_0 = (S_0, V_0, 0, 0, 0, 0)'$ with $S_0 = \frac{(c_2 r_2 + r_1 k_2) \Lambda}{\mu (\mu + c_2 + c_1)}$ and $V_0 = \frac{(k_1 r_2 + c_1 r_1) \Lambda}{\mu (\mu + c_2 + c_1)}$. The basic reproduction number is given from (13) by:

$$\mathcal{R}_c := \frac{N_1 \beta \eta \gamma (a_2 p \sigma + k_4 q)}{N_0 k_3 k_4 k_5} + \frac{N_1 \beta p \gamma}{N_0 k_3 k_4}, \quad (16)$$

where $N_1 = S_0 + \phi_1 V_0$ and $N_0 = S_0 + V_0 = \frac{\Lambda}{\mu}$.

4.3 Stability analysis of the disease-free equilibrium point

Setting $X_1 = (S_1, V_1, E_1, A_1, I_1, R_1)$ where $S_1 = S - S_0$, $V_1 = V - V_0$, $E_1 = E$, $A_1 = A$, $I_1 = I$, and $R_1 = R$, system (10) can be linearized as follows:

$$\frac{\partial X_1}{\partial t}(x, t) = \mathbb{L}(X_1(x, t)) = (\mathbf{A}\Delta + \mathcal{J}(\mathcal{E}_0)) X_1(x, t), \quad (17)$$

where $\mathbf{A} = \text{diag}(\kappa_s, \kappa_v, \kappa_e, \kappa_a, \kappa_i, \kappa_r)$ and

$$\mathcal{J}(\mathcal{E}_0) = \begin{pmatrix} -k_1 & c_2 & 0 & -\beta \frac{S_0}{N_0} & -\beta \eta \frac{S_0}{N_0} & 0 \\ c_1 & -k_2 & 0 & -\beta \frac{\phi V_0}{N_0} & -\phi \beta \eta \frac{\phi V_0}{N_0} & 0 \\ 0 & 0 & -k_3 & \beta \frac{S_0 + \phi V_0}{N_0} & \beta \eta \frac{S_0 + \phi V_0}{N_0} & 0 \\ 0 & 0 & p \gamma & -k_4 & 0 & 0 \\ 0 & 0 & q \gamma & a_2 \sigma & -k_5 & 0 \\ 0 & 0 & 0 & a_1 \sigma & \theta & -\mu \end{pmatrix}.$$

Let us denote by \mathcal{I}_6 the sixth-order identity matrix, $0 = \psi_1 \leq \psi_2 \leq \psi_3 \dots$, the eigenvalues of $-\Delta$ on $\bar{\Sigma}$ with the zero boundary condition, and x an eigenvalue of \mathbb{L} . Then, for all $i \in \mathbb{N}$, the i -characteristic polynomial of the operator \mathbb{L} is given by

$$\begin{aligned}
& \forall i \in \mathbb{N}, \mathcal{P}_{\mathbb{L}}(x) := \det [\mathcal{J}(\mathcal{E}_0) - \psi_i \mathcal{A} - x \mathcal{I}_6] \\
& = \begin{vmatrix} -x - \psi_i \kappa_s - k_1 & c_2 & 0 & -\frac{S_0 \beta}{N_0} & -\frac{S_0 \beta \eta}{N_0} & 0 \\ c_1 & -x - \psi_i \kappa_v - k_2 & 0 & -\frac{V_0 \beta \phi}{N_0} & -\frac{V_0 \beta \eta \phi}{N_0} & 0 \\ 0 & 0 & -x - \kappa_e \psi_i - k_3 & \frac{N_1 \beta}{N_0} & \frac{N_1 \beta \eta}{N_0} & 0 \\ 0 & 0 & p\gamma & -x - \kappa_a \psi_i - k_4 & 0 & 0 \\ 0 & 0 & q\gamma & a_2 \sigma & -x - \kappa_i \psi_i - k_5 & 0 \\ 0 & 0 & 0 & a_1 \sigma & \theta & -x - \psi_i \kappa_r - \mu \end{vmatrix} \\
& = [(-x - \psi_i \kappa_s - k_1)(-x - \psi_i \kappa_v - k_2) - c_1 c_2] \times \\
& \quad \times \begin{vmatrix} -x - \kappa_e \psi_i - k_3 & \frac{N_1 \beta}{N_0} & \frac{N_1 \beta \eta}{N_0} & 0 \\ p\gamma & -x - \kappa_a \psi_i - k_4 & 0 & 0 \\ q\gamma & a_2 \sigma & -x - \kappa_i \psi_i - k_5 & 0 \\ 0 & a_1 \sigma & \theta & -x - \psi_i \kappa_r - \mu \end{vmatrix} \\
& = [(-x - \psi_i \kappa_s - k_1)(-x - \psi_i \kappa_v - k_2) - c_1 c_2] (-x - \psi_i \kappa_r - \mu) \times \\
& \quad \times \begin{vmatrix} -x - \kappa_e \psi_i - k_3 & \frac{N_1 \beta}{N_0} & \frac{N_1 \beta \eta}{N_0} \\ p\gamma & -x - \kappa_a \psi_i - k_4 & 0 \\ q\gamma & a_2 \sigma & -x - \kappa_i \psi_i - k_5 \end{vmatrix} \\
& = (x + \psi_i \kappa_r + \mu) \underbrace{\left[x^2 + (\psi_i \kappa_v + \psi_i \kappa_s + k_2 + k_1) x + (\psi_i^2 \kappa_s + k_1 \psi_i) \kappa_v + k_2 \psi_i \kappa_s + \mu(\mu + c_1 + c_2) \right]}_{g_i^{(1)}(x)} \times \\
& \quad \times \underbrace{\left[x^3 + \varpi_2 x^2 + \varpi_1 x + \varpi_0 \right]}_{g_i^{(2)}(x)}
\end{aligned} \tag{18}$$

where $\varpi_2 = (\kappa_i + \kappa_e + \kappa_a) \psi_i + k_5 + k_4 + k_3$,

$$\begin{aligned}
\varpi_1 &= \frac{1}{a_2 \eta p \sigma + k_4 \eta q + k_5 p} \times \\
& \quad \{ [(\kappa_e + \kappa_a) \kappa_i + \kappa_a \kappa_e] \psi_i + (k_4 + k_3) \kappa_i + (k_5 + k_4) \kappa_e + (k_5 + k_3) \kappa_a \} (a_2 \eta \psi_i p \sigma + k_4 \eta \psi_i q + k_5 \psi_i p) \\
& \quad + (1 - \mathcal{R}_c) (p + \eta q) k_3 k_4 k_5 + (k_4 + k_3) (k_5 + a_2 \eta \sigma) k_5 p + ((k_5 + k_3) k_4 q + k_3 a_2 p \sigma) k_4 \eta \}, \\
\varpi_0 &= \frac{1}{a_2 \eta p \sigma + k_4 \eta q + k_5 p} \times \\
& \quad \{ [\kappa_a \kappa_e \kappa_i \psi_i^2 + ((k_4 \kappa_e + k_3 \kappa_a) \kappa_i + k_5 \kappa_a \kappa_e) \psi_i + (k_3 \kappa_i + k_5 \kappa_e) k_4] (a_2 \eta \psi_i p \sigma + k_4 \eta \psi_i q) \\
& \quad + [\kappa_a \kappa_e \kappa_i \psi_i^2 + ((k_4 \kappa_e + k_3 \kappa_a) \kappa_i + k_5 \kappa_a \kappa_e) \psi_i + (k_4 \kappa_e + k_3 \kappa_a) k_5] \psi_i k_5 p \\
& \quad + k_3 k_5 \kappa_a a_2 \eta \psi_i p \sigma + (1 - \mathcal{R}_c) [a_2 \eta p \sigma + (\kappa_i \psi_i + k_5) p + (\kappa_a \psi_i + k_4) \eta q] k_3 k_4 k_5 \}
\end{aligned}$$

It is clear that for any $i \geq 1$, the roots of $\mathcal{P}_{\mathbb{L}}$ are $x = -\psi_i \kappa_r - \mu$, and those of $g_i^{(1)}$ and $g_i^{(2)}$. Since for $i \geq 1$, $\psi_i \geq 0$, it follows that the roots of $g_i^{(1)}$ have negative real parts.

A rigorous algebraic computation gives:

$$\begin{aligned}
& \varpi_2 \varpi_1 - \varpi_0 \\
&= \frac{1}{a_2 \eta p \sigma + k_4 \eta q + k_5 p} \times \\
& \left\{ q(\psi_i(\eta(\kappa_e(k_3 k_4 k_5(1 - \mathcal{R}_c) + k_4 k_5^2 + (2k_4^2 + k_3 k_4)k_5 + k_4^3 + 2k_3 k_4^2) + (k_4 k_5^2 + (2k_4^2 + 2k_3 k_4)k_5 + 2k_3 k_4^2 + k_5^2 k_4)k_5 \right. \\
& + \eta \kappa_i(k_3 k_4 k_5(1 - \mathcal{R}_c) + (2k_4^2 + k_3 k_4)k_5 + k_4^3 + 2k_3 k_4^2 + k_5^2 k_4)) \\
& + \eta((k_3 k_4 k_5^2 + k_5^2 k_4 k_5)(1 - \mathcal{R}_c) + k_4^2 k_5^2 + (k_4^3 + 2k_3 k_4^2)k_5 + k_3 k_4^3 + k_5^2 k_4^2) \\
& + ((k_4 \kappa_e + k_4 \kappa_a) \eta \kappa_i^2 + (k_4 \kappa_e^2 + 2k_4 \kappa_a \kappa_e + k_4 \kappa_a^2) \eta \kappa_i + (k_4 \kappa_a \kappa_e^2 + k_4 \kappa_a^2 \kappa_e) \eta) \psi_i^3 \\
& + ((k_4^2 + k_3 k_4) \eta \kappa_i^2 + ((2k_4 k_5 + 2k_4^2 + 2k_3 k_4) \kappa_e + (2k_4 k_5 + 2k_4^2 + 2k_3 k_4) \kappa_a) \eta \kappa_i \\
& + ((k_4 k_5 + k_4^2) \kappa_e^2 + (2k_4 k_5 + 2k_4^2 + 2k_3 k_4) \kappa_a \kappa_e + (k_4 k_5 + k_3 k_4) \kappa_a^2) \eta) \psi_i^2 \\
& + p(\psi_i(\kappa_e(k_3 k_4 k_5(1 - \mathcal{R}_c) + k_5^3 + (2k_4 + 2k_3)k_5^2 + (k_4^2 + k_3 k_4)k_5) + \kappa_a(k_3 k_4 k_5(1 - \mathcal{R}_c) + k_5^3 + (2k_4 + 2k_3)k_5^2 \\
& + (k_3 k_4 + k_5^2)k_5) + ((2k_4 + 2k_3)k_5^2 + (k_4^2 + 2k_3 k_4 + k_5^2)k_5) \kappa_i) + (k_3 k_4^2 + k_5^2 k_4)k_5(1 - \mathcal{R}_c) + ((k_5 \kappa_e + k_5 \kappa_a) \kappa_i^2 \\
& + (k_5 \kappa_e^2 + 2k_5 \kappa_a \kappa_e + k_5 \kappa_a^2) \kappa_i + k_5 \kappa_a \kappa_e^2 + k_5 \kappa_a^2 \kappa_e) \psi_i^3 \\
& + ((k_4 + k_3)k_5 \kappa_i^2 + ((2k_5^2 + (2k_4 + 2k_3)k_5) \kappa_e + (2k_5^2 + (2k_4 + 2k_3)k_5) \kappa_a) \kappa_i \\
& + (k_5^2 + k_4 k_5) \kappa_e^2 + (2k_5^2 + (2k_4 + 2k_3)k_5) \kappa_a \kappa_e + (k_5^2 + k_3 k_5) \kappa_a^2) \psi_i^2 + (k_4 + k_3)k_5^3 + (k_4^2 + 2k_3 k_4 + k_5^2)k_5^2 \\
& + p\sigma(\eta(R_c a_2 k_3 k_4 k_5 + (k_4 + k_3)^2 a_2 k_5 + (a_2 k_4 + a_2 k_3)k_5^2 + a_2 k_3 k_4^2 + a_2 k_3^2 k_4) \\
& + ((a_2 \kappa_e + a_2 \kappa_a) \eta \kappa_i^2 + (a_2 \kappa_e^2 + 2a_2 \kappa_a \kappa_e + a_2 \kappa_a^2) \eta \kappa_i + (a_2 \kappa_a \kappa_e^2 + a_2 \kappa_a^2 \kappa_e) \eta) \psi_i^3 \\
& + ((a_2 k_4 + a_2 k_3) \eta \kappa_i^2 + ((2a_2 k_5 + 2a_2 k_4 + 2a_2 k_3) \kappa_e + (2a_2 k_5 + 2a_2 k_4 + 2a_2 k_3) \kappa_a) \eta \kappa_i \\
& + ((a_2 k_5 + a_2 k_4) \kappa_e^2 + (2a_2 k_5 + 2a_2 k_4 + 2a_2 k_3) \kappa_a \kappa_e + (a_2 k_5 + a_2 k_3) \kappa_a^2) \eta) \psi_i^2 \\
& + (((2a_2 k_4 + 2a_2 k_3)k_5 + a_2 k_4^2 + 2a_2 k_3 k_4 + a_2 k_3^2) \eta \kappa_i + ((a_2 k_5^2 + (2a_2 k_4 + 2a_2 k_3)k_5 + a_2 k_4^2 + 2a_2 k_3 k_4) \kappa_e \\
& + (a_2 k_5^2 + (2a_2 k_4 + 2a_2 k_3)k_5 + 2a_2 k_3 k_4 + a_2 k_3^2) \kappa_a) \eta) \psi_i \}
\end{aligned}$$

Thus, $g_i^{(2)}$ meets the Routh-Hurwitz criteria. It then follows that all roots of the characteristic polynomial (18) have negative real parts whenever $\mathcal{R}_c < 1$, which implies that the disease-free equilibrium \mathbb{E}_0 is locally stable (see [41]).

Since $\psi_1 = 0$, it follows that, if $\mathcal{R}_c > 1$,

$$g_1^{(2)}(0) = (1 - \mathcal{R}_c) [a_2 \eta p \sigma + (\kappa_i \psi_i + k_5) p + (\kappa_a \psi_i + k_4) \eta q] k_3 k_4 k_5 < 0 \text{ and } \lim_{x \rightarrow +\infty} g_1^{(2)}(x) = +\infty,$$

which implies that the characteristic polynomial $\mathcal{P}_{\mathbb{L}}$ admits at least one root with positive real part. Thus, the disease-free equilibrium \mathbb{E}_0 is not stable.

The above analysis can be summarized as follows:

Theorem 3. *The disease-free equilibrium \mathbb{E}_0 of the PDE model (10) is locally asymptotically stable in Σ if $\mathcal{R}_c < 1$, and unstable otherwise.*

4.3.1 Global stability of the disease-free equilibrium

Theorem 4. *If $\mathcal{R}_c < 1$, then the disease free equilibrium of the Covid-19 PDE model (10) \mathcal{E}_0 is globally asymptotically stable provided that*

$$\frac{N_1}{N_0} - \frac{(S(x, t) + \phi_1 V(x, t) + \phi_2 R(x, t))}{N(t)} \geq 0. \quad (19)$$

Proof. Let us denote by $(S(x, t), V(x, t), E(x, t), A(x, t), I(x, t), R(x, t))'$ any arbitrary nonnegative solution of Covid-19 IVBP (10)-(11), with $S_0 = \frac{(c_2 r_2 + r_1 k_2) \Lambda}{\mu(\mu + c_2 + c_1)}$ and $V_0 = \frac{(k_1 r_2 + c_1 r_1) \Lambda}{\mu(\mu + c_2 + c_1)}$.

To prove the global asymptotic stability of the disease-free equilibrium $\mathcal{E}_0 = (S_0, V_0, 0, 0, 0, 0)'$, we consider the following Lyapunov functional $\mathcal{K}(t)$ defined as

$$\begin{aligned}\mathcal{K}(S, V, E, A, I, R) &= \int_{\Sigma} \mathcal{Q}(S(x, t), V(x, t), E(x, t), A(x, t), I(x, t), R(x, t)) dx \\ &= \int_{\Sigma} (w'W^{-1}(E, A, I)) dx\end{aligned}$$

where w' is the left eigenvector of the nonnegative matrix $W^{-1}Z$ corresponding to the eigenvalue \mathcal{R}_c . From [23, Proposition 2.1], the time derivative of \mathcal{K} along the nonnegative solution of model (10) is given by

$$\frac{d\mathcal{K}}{dt}(S, V, E, A, I, R) = \int_{\Sigma} [(\mathcal{R}_c - 1)w'(E, A, I) - w'W^{-1}\mathcal{M}(S, V, E, A, I, R)] dx$$

This implies that if $\mathcal{R}_c < 1$, $\frac{d\mathcal{K}}{dt} \leq 0$ whenever $w'W^{-1}\mathcal{M}(S, V, E, A, I, R) \geq \mathbf{0}_{\mathbb{R}^3}$, which is equivalent to the condition $\frac{N_1}{N_0} - \frac{(S(x, t) + \phi_1V(x, t) + \phi_2R(x, t))}{N(t)} \geq 0$. Furthermore, $\frac{d\mathcal{K}}{dt} = 0$ holds if and only if $E = A = I = 0$. Then, $\{\mathcal{E}_0\}$ is the only compact invariant subset of $\left\{ (S, V, E, A, I, R)' \in \mathbb{R}^6 : \frac{d\mathcal{K}}{dt} = 0 \right\}$. By LaSalle's invariance principle [24, 27], if $\mathcal{R}_c < 1$, then the disease-free equilibrium \mathcal{E}_0 of the IBVP (10)-(11) is globally asymptotically stable in Σ provided that condition (19) holds. \square

4.4 Existence of endemic equilibrium points

Let $\mathcal{E} = \mathcal{E}(x) = (S^*, V^*, E^*, A^*, I^*, R^*)'$ any spatially equilibrium of system (10). Thus \mathcal{E} must solve the following system

$$\begin{cases} r_1\Lambda + c_2V^* - k_1S^* - \lambda^*S^* & = 0, \\ r_2\Lambda + c_1S^* - [k_2 + \phi_1\lambda^*]V^* & = 0, \\ \lambda^*(S^* + \phi_1V^* + \phi_2R^*) - k_3E^* & = 0, \\ p\gamma E^* - k_4A^* & = 0, \\ q\gamma E^* + a_2\sigma A^* - k_5I^* & = 0, \\ a_1\sigma A^* + \theta I^* - [\mu + \phi_2\lambda^*]R^* & = 0 \end{cases} \quad (20)$$

Note that algebraic system (20) is equivalent to (6). Thus from [23], we conclude that, as for the ODE Covid-19 model (1):

Proposition 2.

1. If $\mathcal{R}_c < 1$, then the Covid-19 PDE model (1) admits a disease-free equilibrium which can co-exist with two endemic equilibrium points, depending of the sign of coefficients \mathcal{A}_2 and \mathcal{A}_1 of the polynomial (8).
2. If $\mathcal{R}_c > 1$, then the disease-free equilibrium point of the Covid-19 PDE model (1) can coexist with one or three endemic equilibrium points, depending of the sign of coefficients \mathcal{A}_2 and \mathcal{A}_1 of the polynomial (8).

5 Numerical scheme and simulations

In this part of the work, we will construct a numerical scheme to simulate the Coronavirus (COVID-19) spatiotemporal model (10).

5.1 Description of the numerical method

The system of partial differential equations (10) can be numerically solved using the Partial Differential Equation Toolbox in MATLAB[©] (see [42]). Among other things, it can solve systems of equations of the form

$$mu_{tt} + du_t - \nabla \cdot (c \otimes \nabla u) + au = f,$$

using a finite elements approximation. The coefficients m , d , c , a and f are allowed to depend on time, space, and u itself. In our case where $u = (S, V, E, A, I, R)$, we have $m = 0$, $d = 1$, $c = \text{diag}(\kappa_S, \kappa_V, \kappa_E, \kappa_A, \kappa_I, \kappa_R)$, $f = (r_1\Lambda, r_2\Lambda, 0, 0, 0, 0)$ and

$$a(u) = - \begin{pmatrix} -(k_1 + \lambda(u)) & c_2 & 0 & 0 & 0 & 0 \\ c_1 & -(k_2 + \phi_1\lambda(u)) & 0 & 0 & 0 & 0 \\ \lambda(u) & \phi_1\lambda(u) & -k_3 & 0 & 0 & \phi_2\lambda(u) \\ 0 & 0 & p\gamma & -k_4 & 0 & 0 \\ 0 & 0 & q\gamma & a_2\sigma & -k_5 & 0 \\ 0 & 0 & 0 & a_1\sigma & \theta & -(\mu + \phi_2\lambda(u)) \end{pmatrix},$$

where $\lambda(u) = \beta(u_4 + \eta u_5)/(u_1 + u_2 + u_3 + u_4 + u_5 + u_6)$. Together with these coefficients we have to specify boundary conditions (Neumann is the default) and initial values. For the geometry on which to solve the equations we use map data from GADM ([1]), reduced in complexity with the help of Mapshaper ([2]).

5.2 Numerical simulations

In this section provide numerical results of reaction-diffusion model (10). We consider two approaches: (1) all model parameters are constant and (2) the transmission rate coefficient β is time-space dependent. For each case, we present the initial distribution of each variable state at $t = 0$, and the final distribution of each variable state of the model at $t = t_{final}$. Here we assume that $\kappa_s = \kappa_v = \kappa_e = \kappa_a = \kappa_r = 1$ and $\kappa_i = 0.1$, which means that only individuals who have tested positive are confined (or their movements are restricted). Note that we assume that the confinement or the restriction is not perfect, hence $\kappa_i \neq 0$.

5.2.1 Comparison between the ODE model and the PDE models

We begin this part of numerical simulations by comparing the ODE model (1) with the PDE model (12). To this aim, we plot the total number of every variable obtained with the ODE model and the ones obtained with the PDE model in the same panels. Figure 9 displays the total numbers in each compartment for the PDE (blue) and ODE (red) model, as well as the corresponding disease-free equilibrium points (yellow). For the PDE we chose spatially constant parameters and initial values to rule out diffusion effects. From Figure 9, it is obvious that the total numbers in each compartment for the PDE and ODE model coincide.

5.2.2 One peak

For the first test we chose the initial population to be all susceptible to infection, except for one small region in the very south of Germany, where there are also infected, exposed, ... persons. The values are adjusted in such a way that the total number of members in every compartment is the same as before. The results are display in figures 10-15. Figure 10 presents the initial distribution of the model state variables while figures 11-14 display solution of the PDE model after $t_f = 10$ days, $t_f = 250$ days, $t_f = 500$ days, and $t_f = 750$ days, respectively. The total

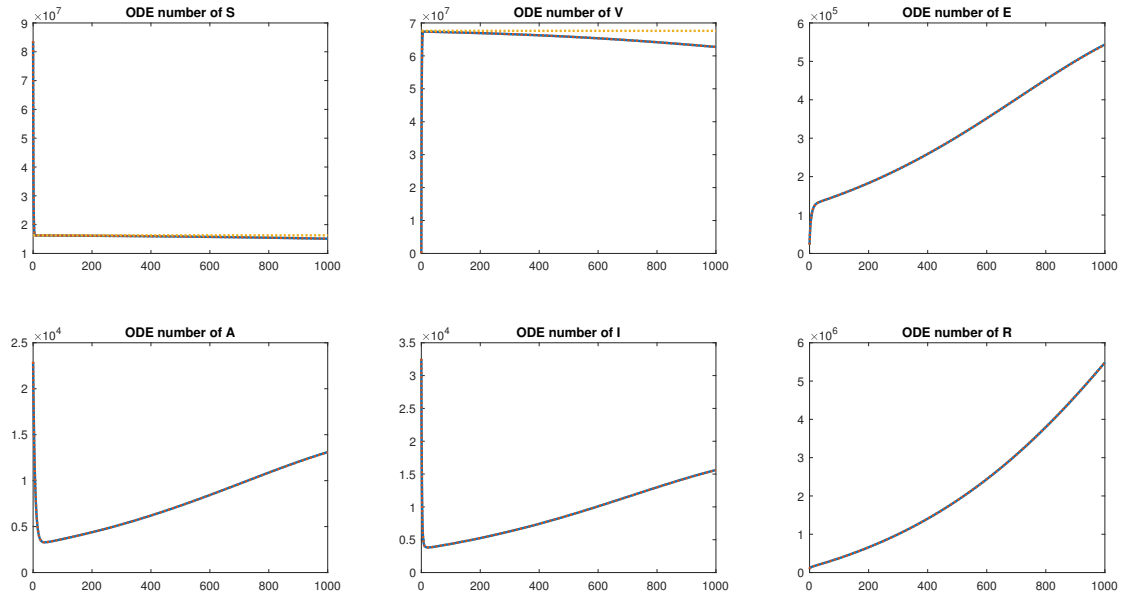


Figure 9: Comparison of the ODE and PDE with spatially constant initial values. In this case the models coincide.

number of members in each compartment over time (blue), compared to the ODE model (red) and the disease-free state (yellow), is displayed in Figure 15.

5.2.3 Two peaks

For the next test we added a second peak in western Germany, close to Aachen/Heinsberg, where a major outbreak of Covid occurred in early 2020. Again, the total numbers of members in each compartment did not change. The results are display in Figures 16-21. Figure 16 presents the initial distribution of model state variables while Figures 11-20 display the solution of the PDE model after $t_f = 10$ days, $t_f = 250$ days, $t_f = 500$ days, and $t_f = 750$ days, respectively. The total number of members in each compartment over time (blue), compared to the ODE model (red) and the disease-free state (yellow) is displayed in figure 21.

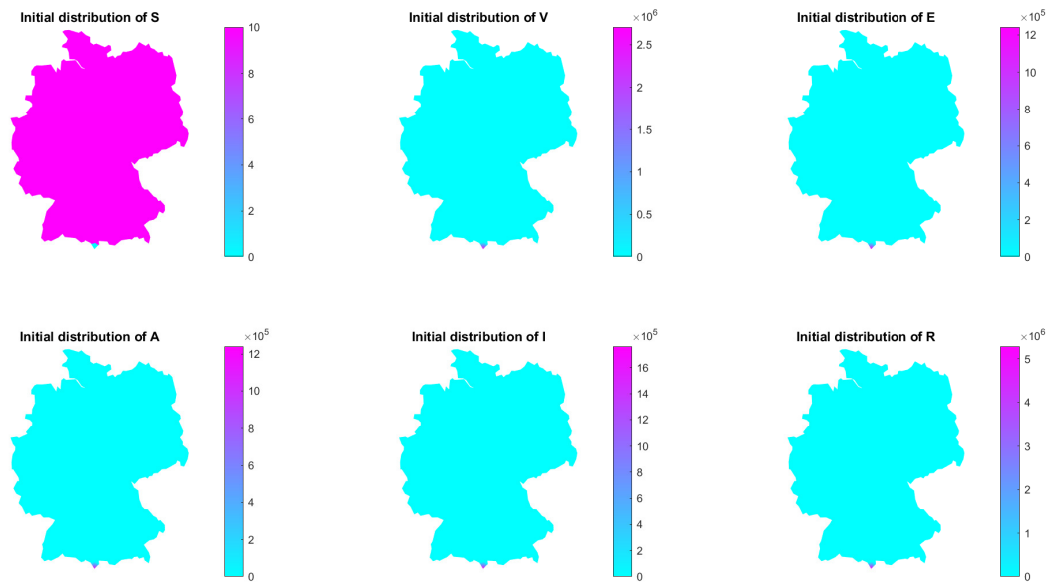


Figure 10: Initial distribution of model state variables where there is one peak in the south.

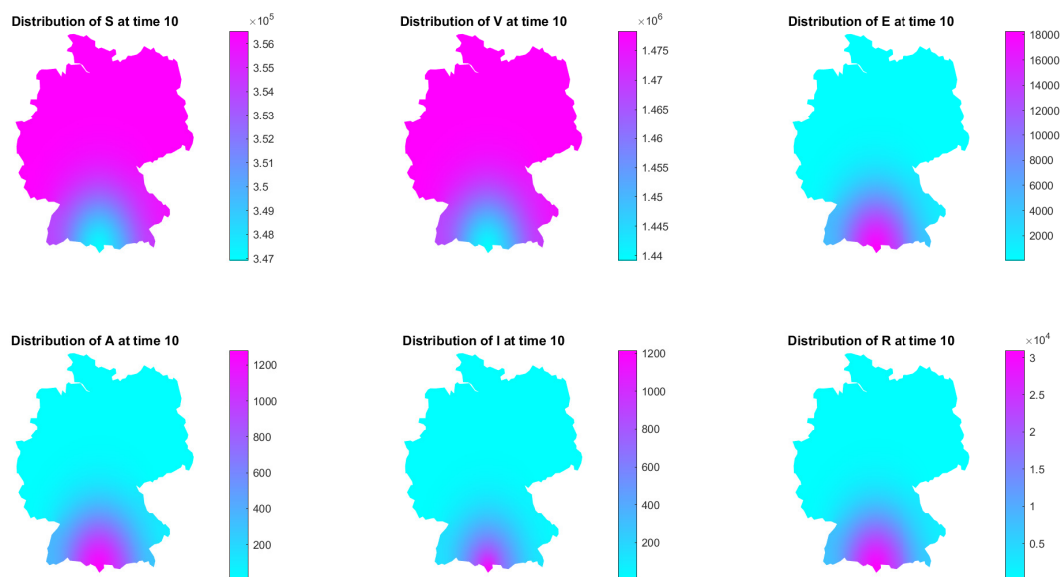


Figure 11: Solution after $t_f = 10$ days.

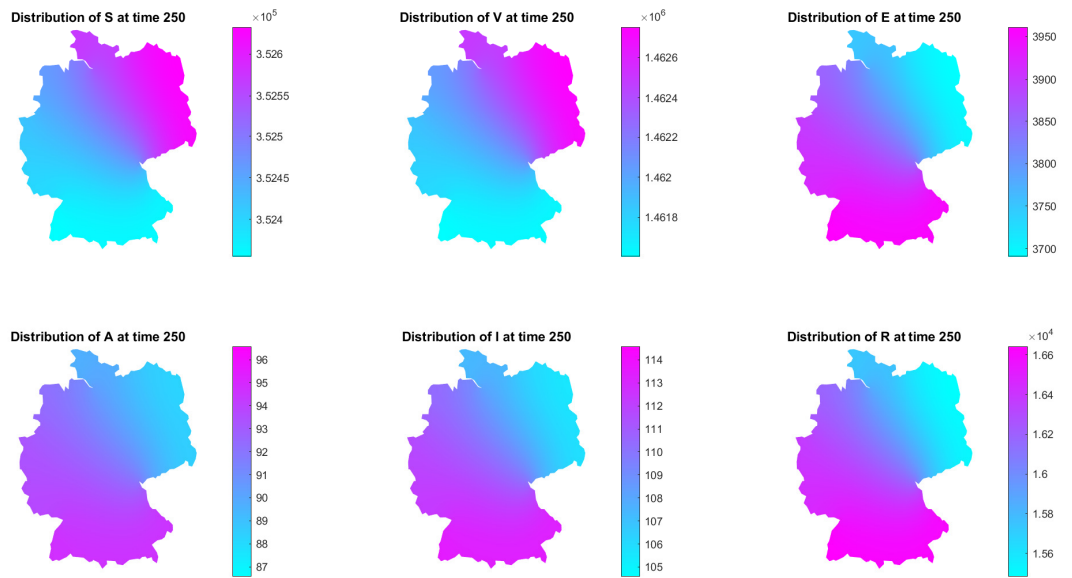


Figure 12: Solution after $t_f = 250$ days.

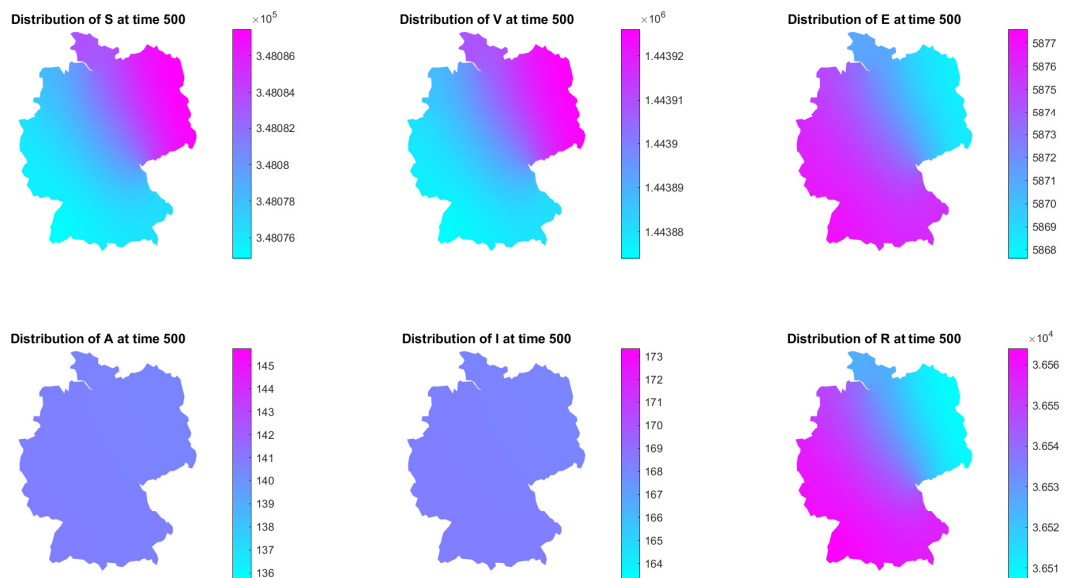


Figure 13: Solution after $t_f = 500$ days.

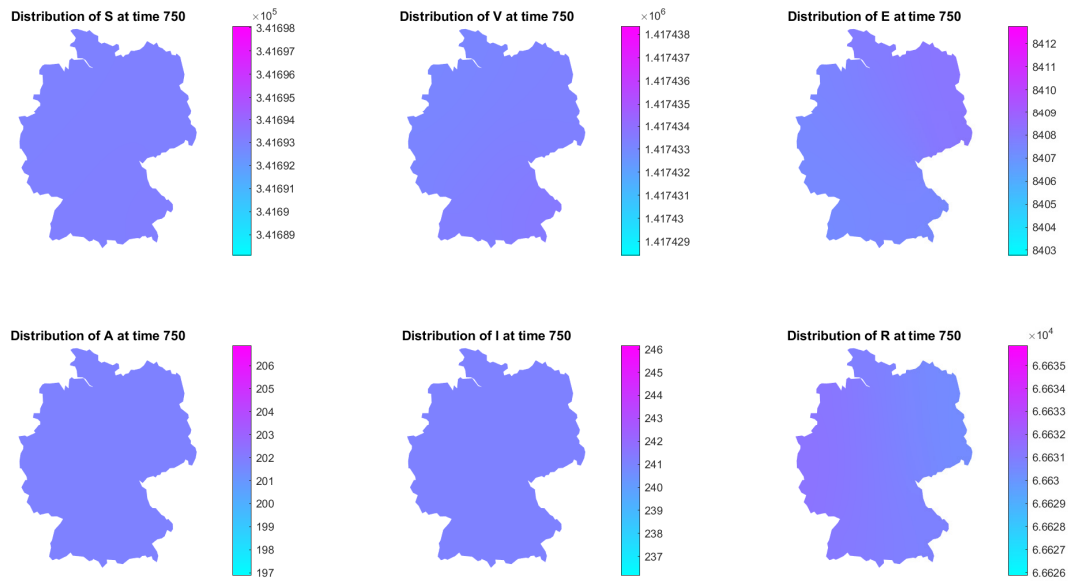


Figure 14: Solution after $t_f = 750$ days.

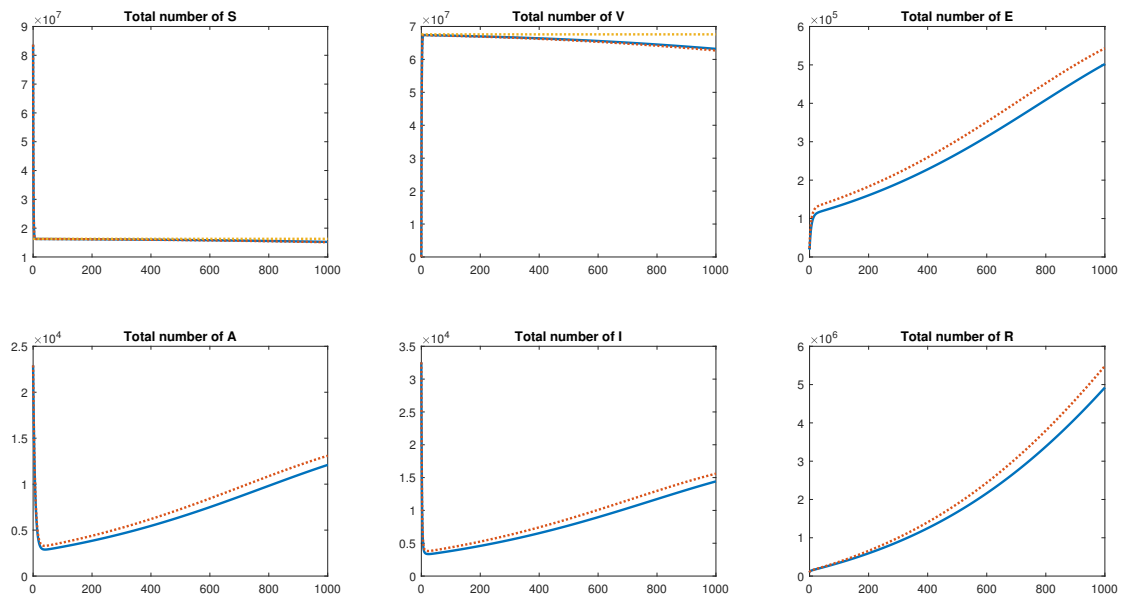


Figure 15: Total number of members in each compartment over time (blue), compared to the ODE model (red) and the disease-free state (yellow).

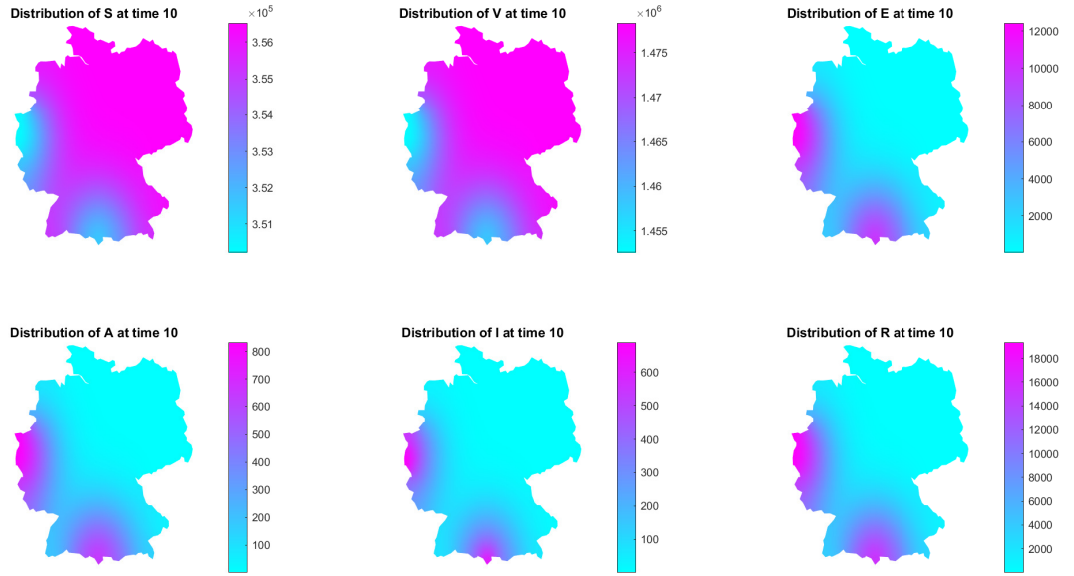


Figure 17: Solution after $t_f = 10$ days.

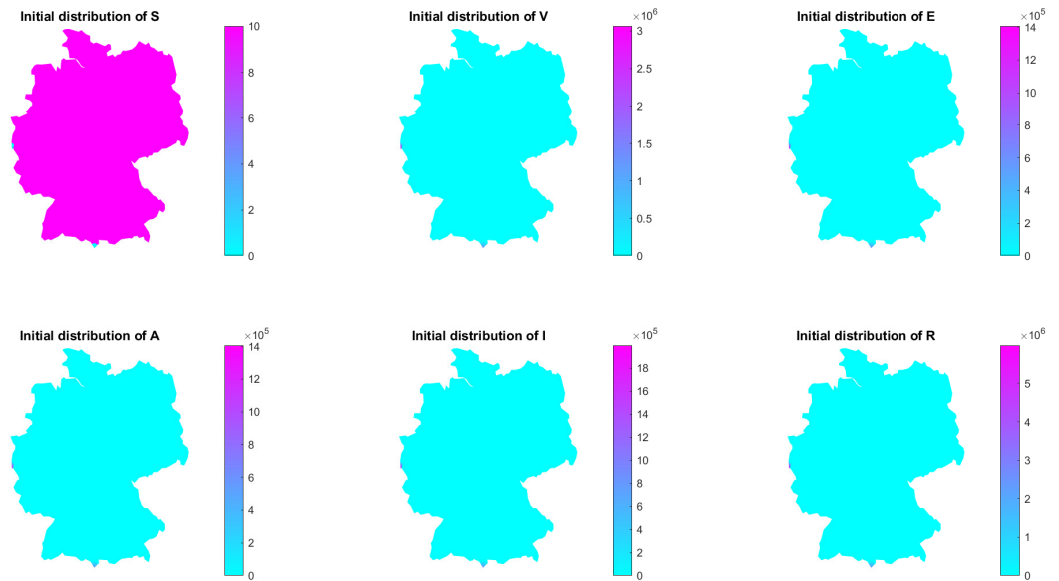


Figure 16: Initial distribution of model state variables where there are two peaks (south and west).

5.2.4 Bavaria

Figures 22-28 display a series of images where only the state of Bavaria holds exposed, asymptomatic infected, and symptomatic infected individuals. Initial distribution of model state variables are displayed on figures 22, while solution after $t_f = 10$ days, $t_f = 250$ days, $t_f = 500$ days, $t_f = 750$ days, and $t_f = 1000$ days, respectively, are display in figure 23-27. We see that

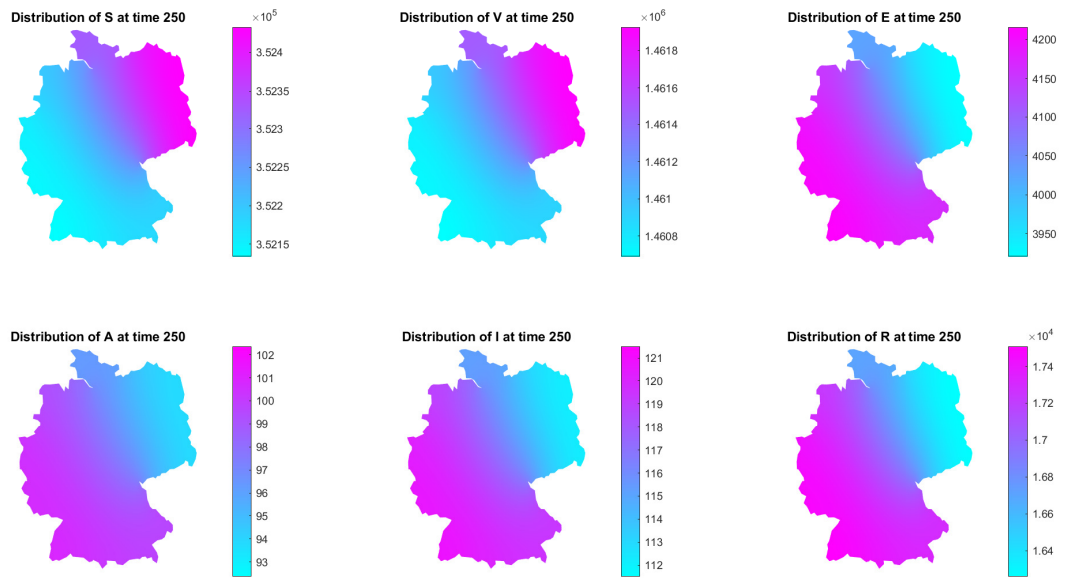


Figure 18: Solution after $t_f = 250$ days.

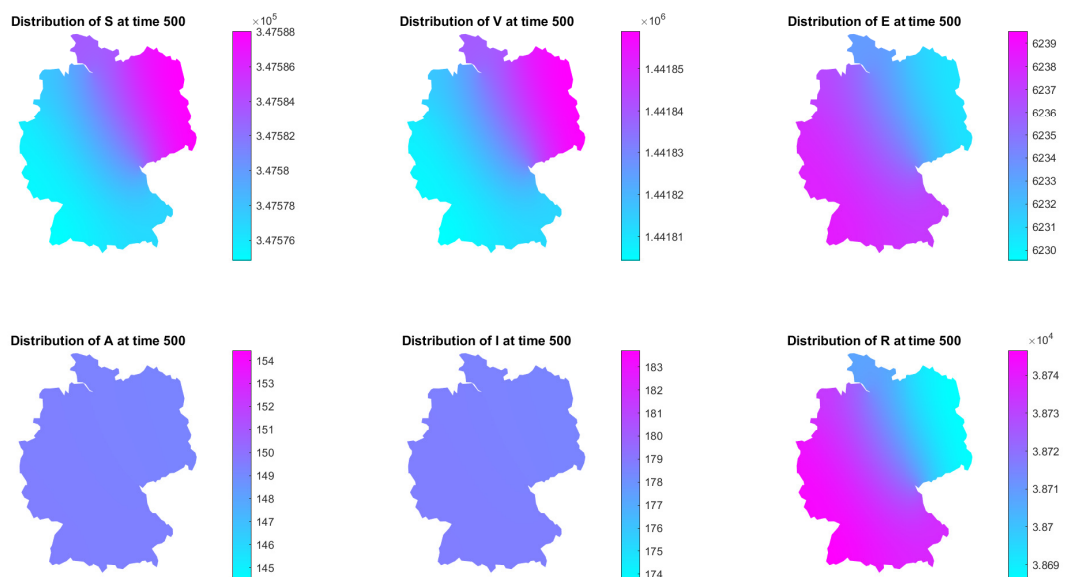


Figure 19: Solution after $t_f = 500$ days.

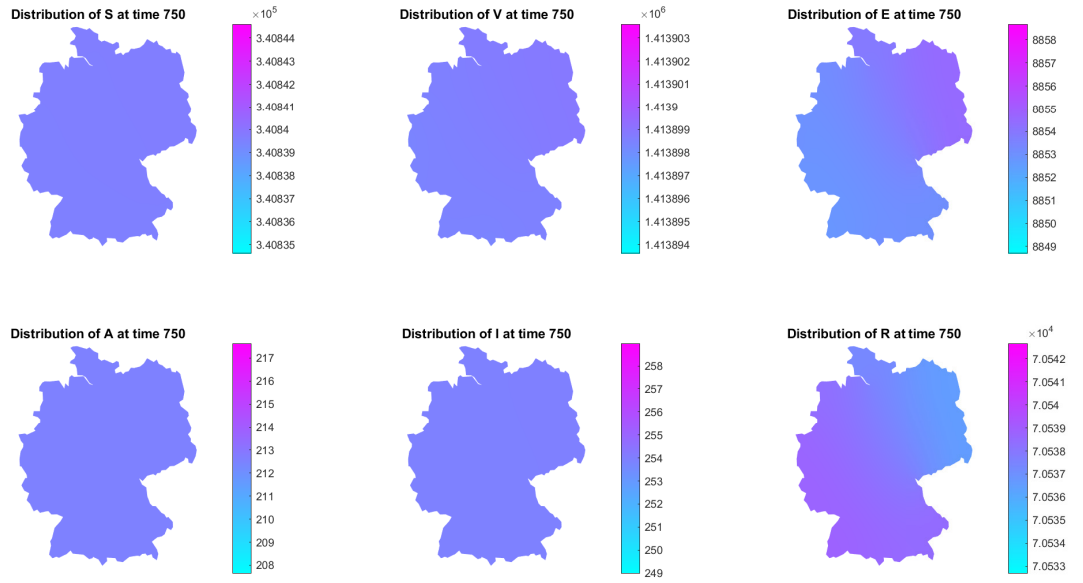


Figure 20: Solution after $t_f = 750$ days.

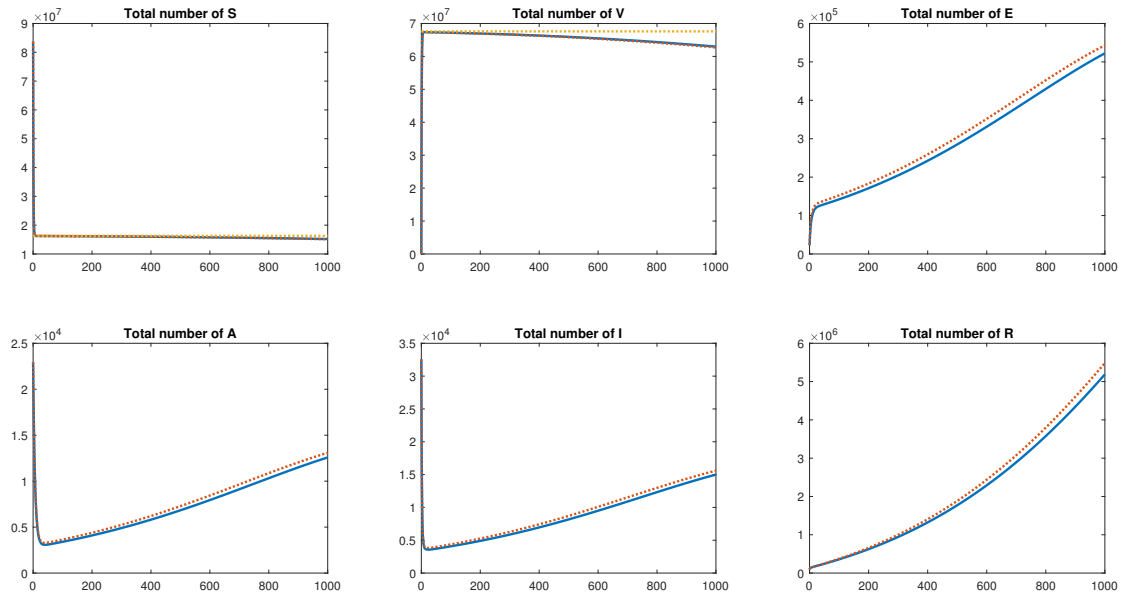


Figure 21: Total number of members in each compartment over time (blue), compared to the ODE model (red) and the disease-free state (yellow).

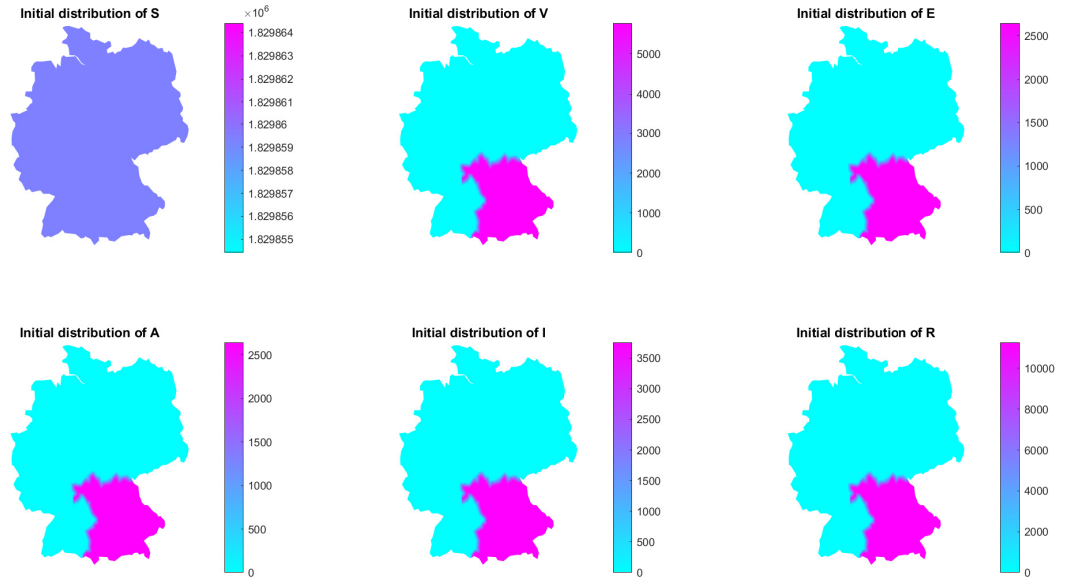


Figure 22: Initial distribution of model state variables where only the state of Bavaria holds exposed, asymptomatic infected, and symptomatic infected individuals.

more time passes, the more the infection spreads to the rest of the country. Note that the total numbers in each compartment are slightly different to the ones before, this is because MATLAB smoothes out the initial value along the Bavarian border. The total number of members in each compartment over time (blue), compared to the ODE model (red) and the disease-free state (yellow), is displayed in Figure 28.

5.2.5 Time-dependent parameters

There has been proved that temperature plays an important role in the Covid-19 spread in Germany [17]. To take this into account, we suppose that the transmission rate coefficient β is time-dependent. We choose for this case $\beta(t) = \beta_{crit} + 0.1 \cos(0.01 * t)$, where $\beta_{crit} = 0.819792192423568$ is the critical value of β for which there is $\mathcal{R}_c = 1$. Figures 29-32 illustrate the distribution of model states when the final time t_{final} is equal to 10, 250, 500 and 750 days, respectively. Note that for $t_{final} = 750$ days (see figure 32), the transmission rate β is equal to 0.8544557242070706, which corresponds to a value of the control reproduction number greater than one ($\mathcal{R}_c = 1.042283315337544$); While for $t_{final} = 3299$ days, we obtain β equal to 0.8194644792794378 less than β_{crit} , and which corresponds to a value of the control reproduction number less than one ($\mathcal{R}_c = 0.9996002485176618$). This can be interpreted by the fact that it will take a long time for the existing control measures to assure the eradication of the coronavirus disease. Indeed, the forecasting (see figure 3) indicates that over than 2000 days are needed to have the number of detected case close to zero.

The total number of members in each compartment over time (blue), compared to the ODE model (red) and the disease-free state (yellow) when $\beta(t) = \beta_{crit} + 0.1 \cos(0.01 * t)$ is depicted in figure 33.

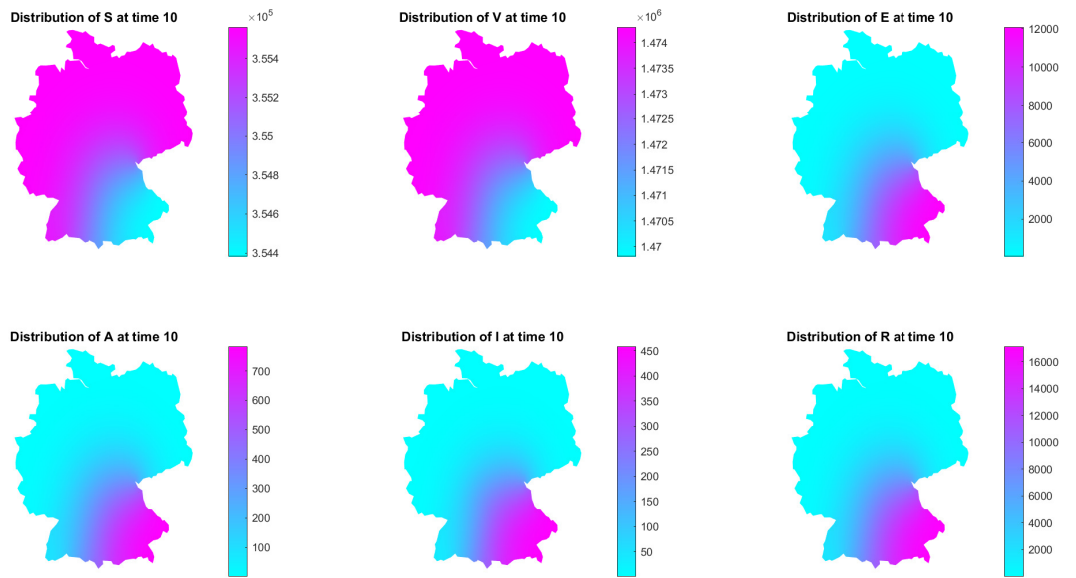


Figure 23: Solution after $t_f = 10$ days.

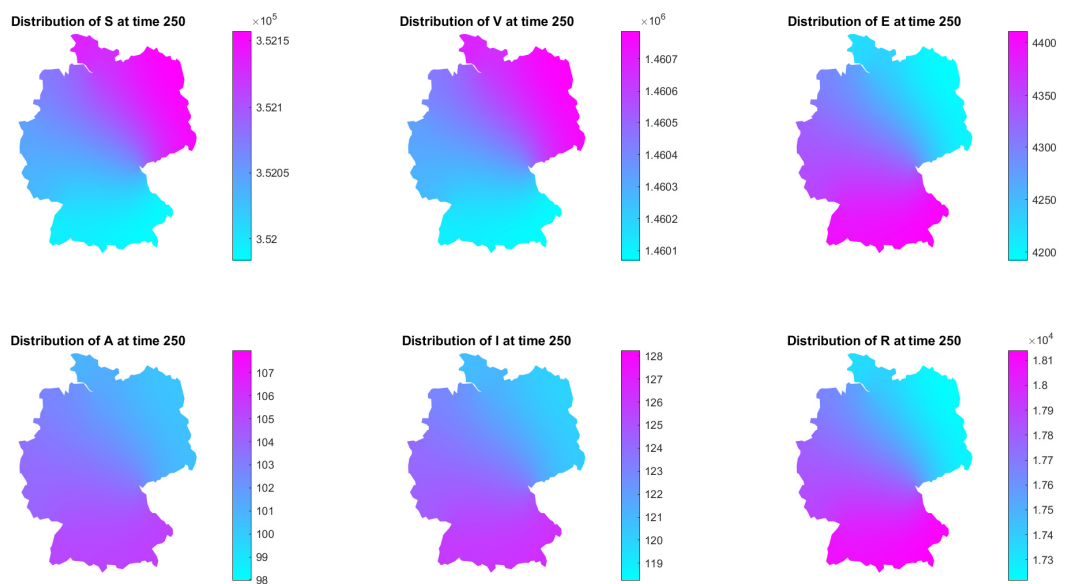


Figure 24: Solution after $t_f = 250$ days.

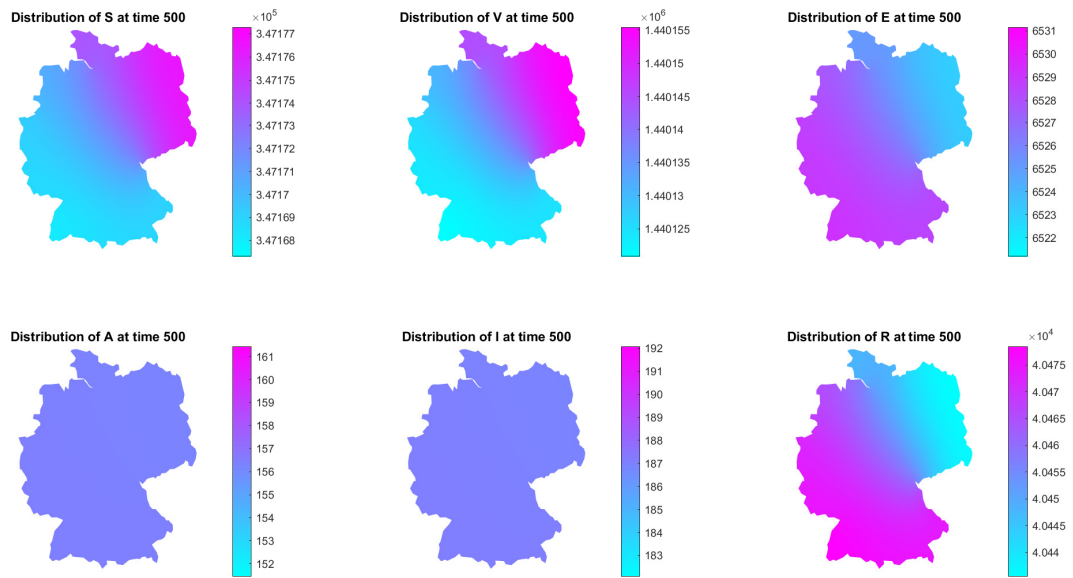


Figure 25: Solution after $t_f = 500$ days.

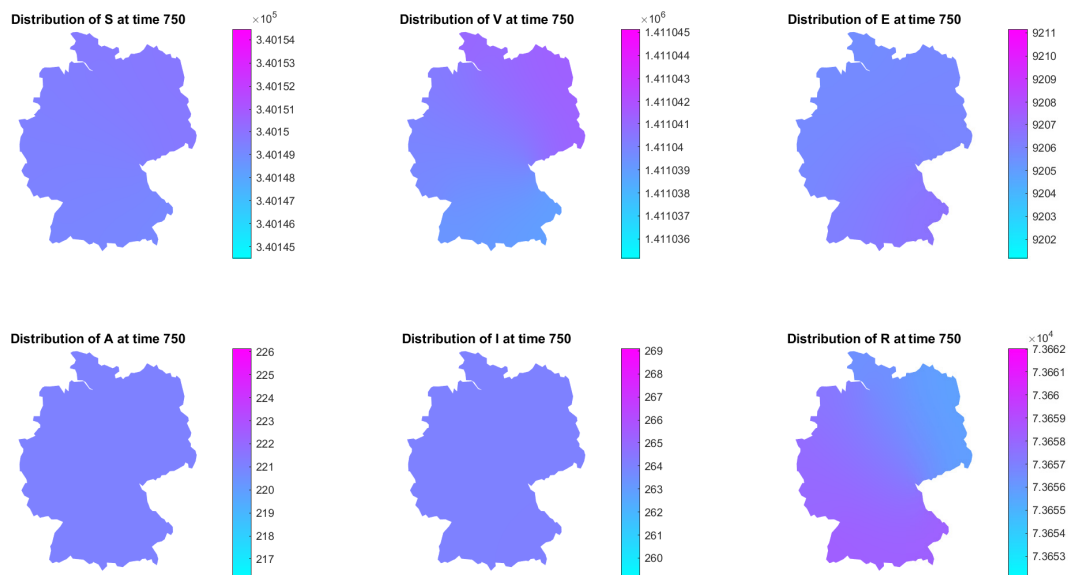


Figure 26: Solution after $t_f = 750$ days.

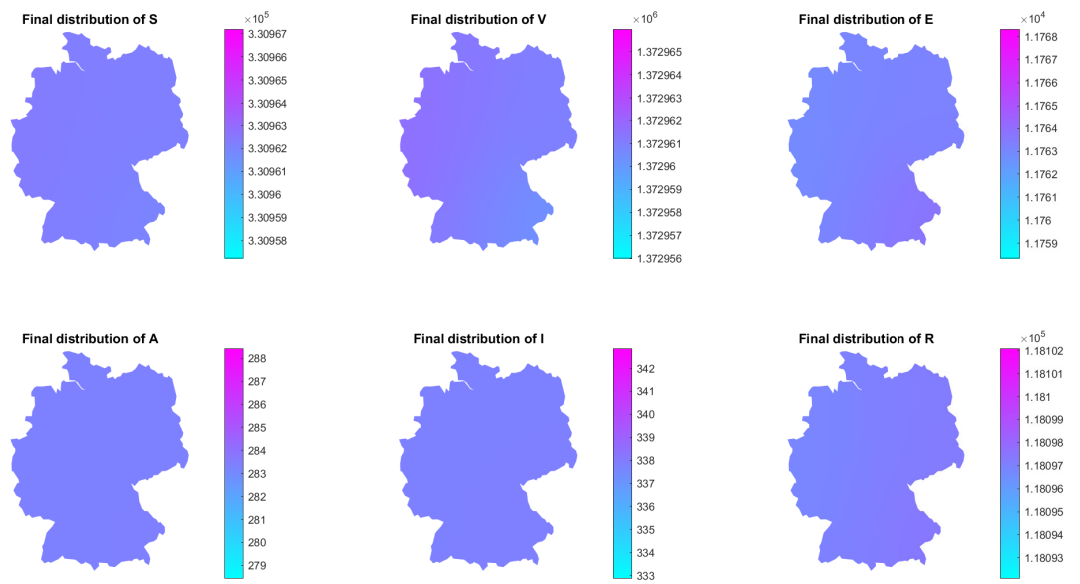


Figure 27: Final state of the solution after $t_f = 1000$ days.

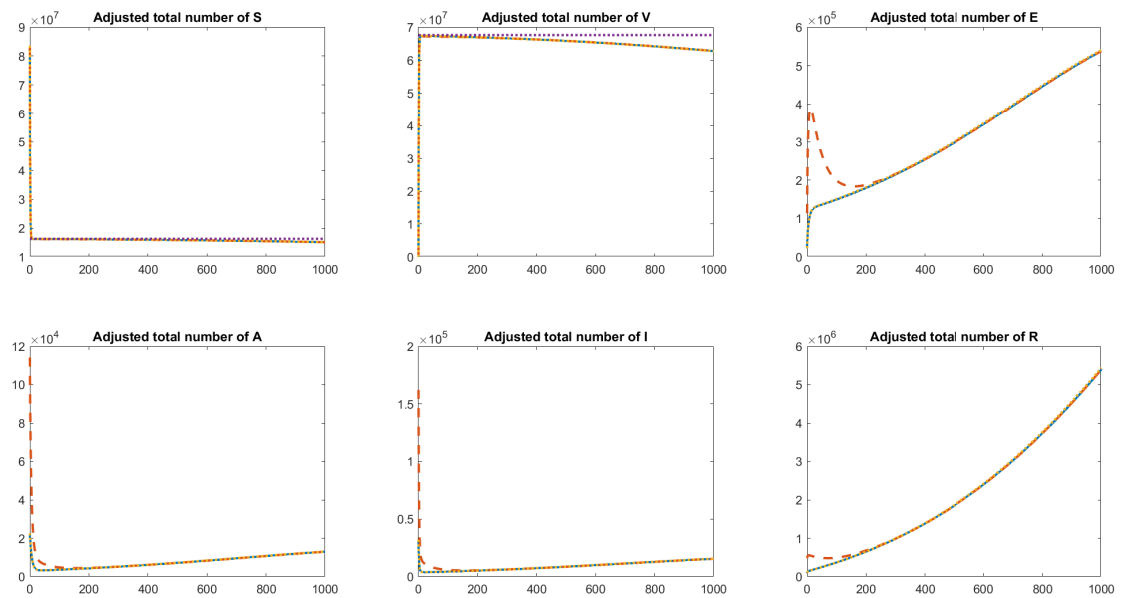


Figure 28: Total number of members in each compartment over time (blue), compared to the numbers only in Bavaria adjusted for size (red), the ODE model (yellow) and the disease-free state (purple).

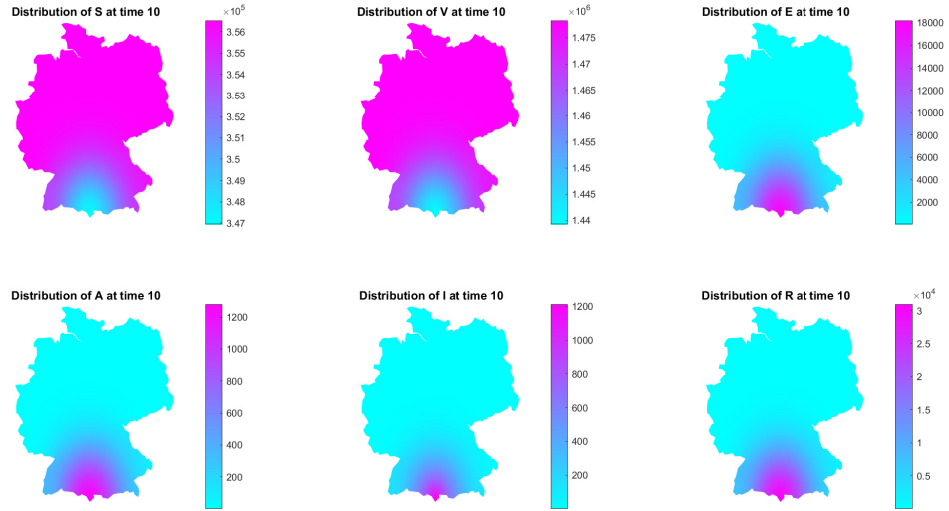


Figure 29: Final distribution of model state variables when all parameter values are ones of Table 1 except $\beta(t) = \beta_{crit} + 0.1 \cos(0.01 * t)$, where $\beta_{crit} = 0.819792192423568$ is the critical value of β for which there is $\mathcal{R}_c = 1$ with $t_{final} = 10$ days.

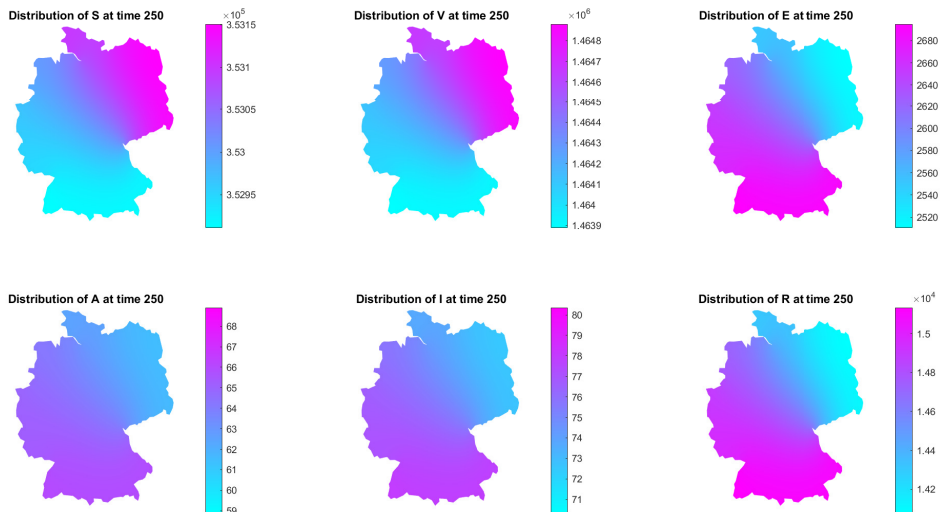


Figure 30: Final distribution of model state variables when all parameter values are ones of Table 1 except $\beta(t) = \beta_{crit} + 0.1 \cos(0.01 * t)$, where $\beta_{crit} = 0.819792192423568$ is the critical value of β for which there is $\mathcal{R}_c = 1$ with $t_{final} = 250$ days.

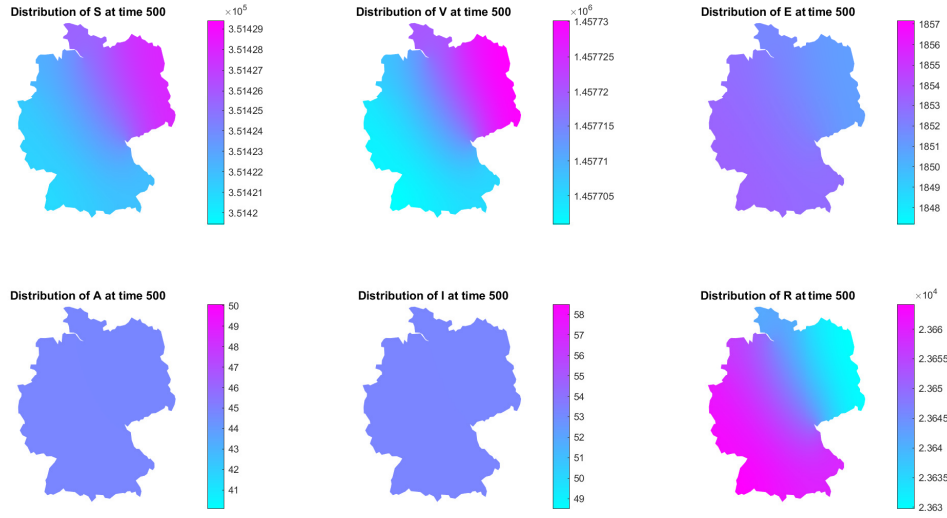


Figure 31: Final distribution of model state variables when all parameter values are ones of Table 1 except $\beta(t) = \beta_{crit} + 0.1 \cos(0.01 * t)$, where $\beta_{crit} = 0.819792192423568$ is the critical value of β for which there is $\mathcal{R}_c = 1$ with $t_{final} = 500$ days.

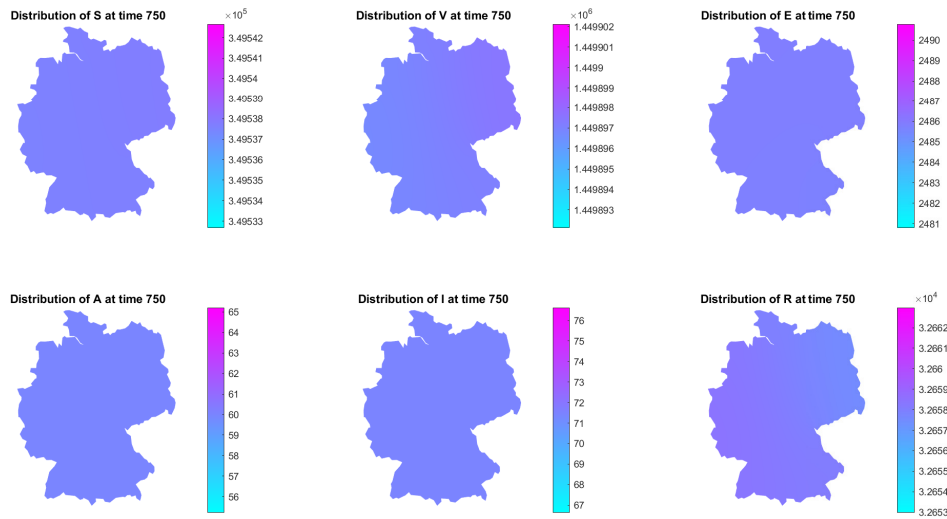


Figure 32: Final distribution of model state variables when all parameter values are ones of Table 1 except $\beta(t) = \beta_{crit} + 0.1 \cos(0.01 * t)$, where $\beta_{crit} = 0.819792192423568$ is the critical value of β for which there is $\mathcal{R}_c = 1$ with $t_{final} = 750$ days.

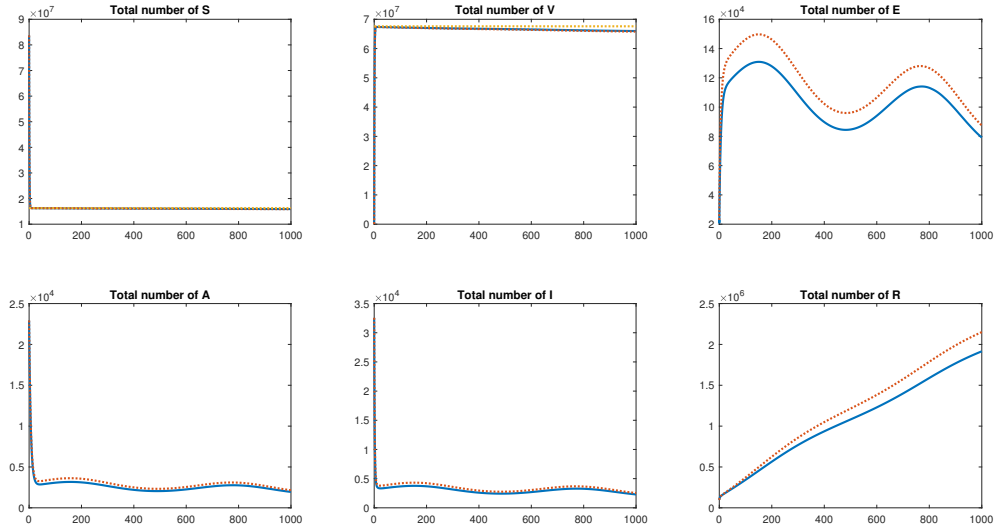


Figure 33: Total number of members in each compartment over time (blue), compared to the ODE model (red) and the disease-free state (yellow). All parameter values are ones of Table 1 except $\beta(t) = \beta_{crit} + 0.1 \cos(0.01 * t)$, where $\beta_{crit} = 0.819792192423568$ is the critical value of β for which there is $\mathcal{R}_c = 1$.

6 Conclusion and perspectives

In this work, we formulated two Covid-19 transmission dynamics models first using ordinary differential equations, and secondly, partial differential equations (reaction-diffusion model). For both models, we computed the control reproduction number and proved the global asymptotic stability of the disease-free equilibrium point whenever the control reproduction number is less than one. We also proved that both models admit at least one endemic equilibrium point whenever the control reproduction number is greater than one, which implies that the disease-free equilibrium becomes unstable. Using the daily infected reported cases in Germany from December 31, 2020, to February 28, 2021, we calibrated the ODE model by estimated model parameters. We found that the control reproduction number is approximately equal to 1.13 which confirms that, even if the vaccination level is high, Covid-19 will be present in the country, and this for the next years. To determine key parameters which influence the model dynamics, we performed a global sensitivity analysis by computing partial rank correlation coefficients between model parameters and the control reproduction number (respectively model state variables). It follows that the parameters β , σ , Λ , and γ are the most important parameters to influence the disease dynamics.

The final part of the work concerns numerical studies. After presenting the numerical method use to simulate the models, we performed various numerical simulations to validate our theoretical results. Indeed, several cases are considered: First of all, we considered the case when all parameters are constant, with different final times, followed by the case when the transmission rate coefficient β is time-dependent. Thirdly, we considered the case in which the initial population is entirely susceptible to infection, except for one small region in the very south of Germany, where there are also infected, exposed, ... persons, and the case when we added a second peak in western Germany. These two cases were followed by the case when only the state of Bavaria holds exposed, asymptomatic infected, and symptomatic infected individuals. For each of the above cases, we compared the ODE model with the PDE model by drawing in

the same panel the total numbers in each compartment for the PDE and ODE model, as well as the corresponding disease-free equilibrium points (yellow). In order to directly compare the two models, we chose spatially constant parameters and initial values for the PDE to rule out diffusion effects. This permits to conclude that the total numbers in each compartment for the PDE and ODE model coincide in this case, and in a quantitative point of view, the ODE model and the PDE model then give the same results.

In the present study, we did not take into account the fact that model parameters can depend on time and space. Indeed, the transmission rate β , for example, should not be the same in a country as Germany which has sixteen federal states with different population sizes and densities. Thus, estimating some model parameters for each German state, taking into account population movement between each state, constitutes a direct perspective of this work.

Acknowledgment

The authors thank the Ministry of Science, Research and the Arts of the State of Baden-Württemberg (Ministerium für Wissenschaft, Forschung und Kunst Baden-Württemberg) for the grant supporting a joint research project within the 2022 initiative "Science Cooperation Africa (2021/2022)" which permitted the first author to have a research stay at the Department of Mathematics and Statistics of the University of Konstanz, Germany. The first author also thanks the Zukunftskolleg for providing him with all the necessary logistics during this research stay at the University of Konstanz.

Conflict of interest

The authors declare that they have no conflict of interest.

References

- [1] GADM. https://gadm.org/download_country_v3.html, Accessed 27-03-2023.
- [2] Mapshaper. <https://mapshaper.org>, Accessed 27-03-2023.
- [3] Hamadjam Abboubakar, Jean Claude Kamgang, Léontine Nkague Nkamba, and Daniel Tieudjo. Bifurcation thresholds and optimal control in transmission dynamics of arboviral diseases. *Journal of Mathematical Biology*, 76(1-2):379–427, 2018.
- [4] Hamadjam Abboubakar and Reinhard Racke. Mathematical modeling of the coronavirus (covid-19) transmission dynamics using classical and fractional derivatives. *Konstanzer Schriften Math., University of Konstanz*, Konstanzer Schriften Math. 407, 2022.
- [5] Aniruddha Adiga, Devdatt Dubhashi, Bryan Lewis, Madhav Marathe, Srinivasan Venkatramanan, and Anil Vullikanti. Mathematical models for covid-19 pandemic: a comparative analysis. *Journal of the Indian Institute of Science*, 100(4):793–807, 2020.
- [6] Nauman Ahmed, Amr Elsonbaty, Ali Raza, Muhammad Rafiq, and Waleed Adel. Numerical simulation and stability analysis of a novel reaction–diffusion covid-19 model. *Nonlinear Dynamics*, 106(2):1293–1310, 2021.

- [19] Shuyu Han, Chengxia Lei, and Xiaoyan Zhang. Qualitative analysis on a diffusive sirs epidemic model with standard incidence infection mechanism. *Zeitschrift für Angewandte Mathematik und Physik*, 71(6):1–23, 2020.
- [20] Hannah, Ritchie and Edouard, Mathieu and Lucas, Rodés-Guirao and Cameron, Appel and Charlie, Giattino and Esteban, Ortiz-Ospina and Joe, Hasell and Bobbie, Macdonald and Saloni, Dattani and Max, Roser. Coronavirus pandemic (covid-19). <https://ourworldindata.org/coronavirus>, Accessed March, 28 2022.
- [21] Xingjie Hao, Shanshan Cheng, Degang Wu, Tangchun Wu, Xihong Lin, and Chaolong Wang. Reconstruction of the full transmission dynamics of covid-19 in wuhan. *Nature*, 584(7821):420–424, 2020.
- [22] Priyanka Harjule, Vinita Tiwari, and Anupam Kumar. Mathematical models to predict covid-19 outbreak: An interim review. *Journal of Interdisciplinary Mathematics*, 24(2):259–284, 2021.
- [23] Khalid Hattaf and Noura Yousfi. Global stability for reaction–diffusion equations in biology. *Computers & Mathematics with Applications*, 66(8):1488–1497, 2013.
- [24] Daniel Henry. *Geometric theory of semilinear parabolic equations*, volume 840. Springer, 2006.
- [25] Lyndon P James, Joshua A Salomon, Caroline O Buckee, and Nicolas A Menzies. The use and misuse of mathematical modeling for infectious disease policymaking: lessons for the covid-19 pandemic. *Medical Decision Making*, 41(4):379–385, 2021.
- [26] Panayotis G Kevrekidis, Jesús Cuevas-Maraver, Yannis Drossinos, Zoi Rapti, and George A Kevrekidis. Reaction-diffusion spatial modeling of covid-19: Greece and andalusia as case examples. *Physical Review E*, 104(2):024412, 2021.
- [27] Joseph P La Salle. *The stability of dynamical systems*. SIAM, 1976.
- [28] Macrotrends. Germany life expectancy 1950-2022. <https://www.macrotrends.net/countries/DEU/germany/life-expectancy>, Accessed June, 09 2022.
- [29] Youcef Mammeri. A reaction-diffusion system to better comprehend the unlockdown: Application of seir-type model with diffusion to the spatial spread of covid-19 in france. *Computational and Mathematical Biophysics*, 8(1):102–113, 2020.
- [30] Simeone Marino, Ian B Hogue, Christian J Ray, and Denise E Kirschner. A methodology for performing global uncertainty and sensitivity analysis in systems biology. *Journal of Theoretical Biology*, 254(1):178–196, 2008.
- [31] Xavier Mora. Semilinear parabolic problems define semiflows on c^k spaces. *Transactions of the American Mathematical Society*, 278(1):21–55, 1983.
- [32] Samuel Mwalili, Mark Kimathi, Viona Ojiambo, Duncan Gathungu, and Rachel Mbogo. Seir model for covid-19 dynamics incorporating the environment and social distancing. *BMC Research Notes*, 13(1):1–5, 2020.
- [33] Khondoker Nazmoon Nabi, Hamadjam Abboubakar, and Pushpendra Kumar. Forecasting of covid-19 pandemic: From integer derivatives to fractional derivatives. *Chaos, Solitons & Fractals*, 141:110283, 2020.

- [34] World Health Organization et al. Coronavirus disease 2019 (covid-19): situation report, 82. *World Health Organization*, 2020.
- [35] Our World in Data. Coronavirus (covid-19) vaccinations. <https://ourworldindata.org/covid-vaccinations>, Accessed June, 09 2022.
- [36] An Pan, Li Liu, Chaolong Wang, Huan Guo, Xingjie Hao, Qi Wang, Jiao Huang, Na He, Hongjie Yu, Xihong Lin, et al. Association of public health interventions with the epidemiology of the covid-19 outbreak in wuhan, china. *Jama*, 323(19):1915–1923, 2020.
- [37] Rui Peng and Xiao-Qiang Zhao. A reaction–diffusion sis epidemic model in a time-periodic environment. *Nonlinearity*, 25(5):1451, 2012.
- [38] Iman Rahimi, Fang Chen, and Amir H Gandomi. A review on covid-19 forecasting models. *Neural Computing and Applications*, pages 1–11, 2021.
- [39] Zhisheng Shuai and Pauline van den Driessche. Global stability of infectious disease models using lyapunov functions. *SIAM Journal on Applied Mathematics*, 73(4):1513–1532, 2013.
- [40] Joel Smoller. Shock waves and reaction-diffusion equations. *Grundlehren math. Wiss.*, 258, 1983.
- [41] Calvin Tadmon and Severin Foko. A transmission dynamics model of covid-19: Case of cameroon. *Infectious Disease Modelling*, 2022.
- [42] The MathWorks Inc. Partial Differential Equation Toolbox. <https://mathworks.com/products/pde.html>, Accessed 27-03-2023.
- [43] Mustafa Turkyilmazoglu. Indoor transmission of airborne viral aerosol with a simplistic reaction-diffusion model. *The European Physical Journal Special Topics*, pages 1–11, 2022.
- [44] Pauline Van den Driessche and James Watmough. Reproduction numbers and sub-threshold endemic equilibria for compartmental models of disease transmission. *Mathematical Biosciences*, 180(1-2):29–48, 2002.
- [45] W. Walter. *Ordinary Differential Equations*. Springer, 1998.
- [46] World Health Organization (WHO). Status of Covid-19 Vaccines within WHO EUL/PQ evaluation process. https://en.wikipedia.org/wiki/List_of_COVID-19_vaccine_authorizations, Accessed 27-07-2022.
- [47] Jianyong Wu, Radhika Dhingra, Manoj Gambhir, and Justin V Remais. Sensitivity analysis of infectious disease models: methods, advances and their application. *Journal of The Royal Society Interface*, 10(86):20121018, 2013.
- [48] Joseph T Wu, Kathy Leung, and Gabriel M Leung. Nowcasting and forecasting the potential domestic and international spread of the 2019-ncov outbreak originating in wuhan, china: a modelling study. *The Lancet*, 395(10225):689–697, 2020.
- [49] Cheng-Cheng Zhu and Jiang Zhu. Dynamic analysis of a delayed covid-19 epidemic with home quarantine in temporal-spatial heterogeneous via global exponential attractor method. *Chaos, Solitons & Fractals*, 143:110546, 2021.